ADVANCED PHYSICS RESEARCH
Open Access
www.advphysicsres.com

Terahertz Metasurfaces for Polarization Manipulation and Detection: Principles and Emerging Applications

Yongliang Liu, Yifei Xu, Bo Yu, Wenwei Liu, Zhengren Zhang, Hua Cheng,* and Shuqi Chen**

Terahertz frequencies locating between microwave and infrared regions can record and process optical information for next-generation information technology such as 6G communication. Metasurfaces, as emerging planar optical components built with micro- or nanostructures, enable precise control, and manipulation of electromagnetic waves from near fields to far fields. These subwavelength artificial structures can be engineered to exhibit specific polarization responses, thus holding significant potential for applications in polarization detection. In the terahertz (THz) region, polarization information is crucial for identifying and analyzing the properties of materials in the terahertz. In this review, we focus on recent advances in terahertz metasurfaces for polarization manipulation and detection, including principles and emerging applications. New polarization detection methods such as polarization state conversion, polarization-selective absorption, polarization-selective focusing, and vector beam construction are discussed. Finally, it is concluded with a few perspectives on emerging trends and existing challenges in the fields of terahertz polarization manipulation and detection.

1. Introduction

Lying between the infrared and millimeter wave regimes, the terahertz frequency (0.1–10 THz) band is commonly denoted as the "terahertz gap", which is characterized as low photon energy, wide band, and high transparency.[1–3] One of the most intriguing applications of terahertz waves is biochemical sensing, because most of the collective vibrational modes of biological macromolecules are located in the terahertz range, and the chiral spectra in the visible and infrared light range often lack distinguishable fingerprint specificity.[4] Traditional terahertz biochemical sensing techniques are mostly combined with terahertz absorption spectroscopy. However, traditional terahertz absorption spectroscopy measures the single-polarized amplitude and phase changes in the terahertz band, making it difficult to capture the complete polarization and chirality information that is vital to analyze structural biochemical materials.[5,6]

Polarization, as a key attribute of electromagnetic (EM) waves, carries essential information about EM waves.[7–10] The polarization of light provides a pathway for a deeper understanding of light-matter interactions. The manipulation and detection of polarization states play essential roles in modern optics, and have been widely applied in astronomy,[11–14] remote sensing,[15] biology,[16] medicine,[17] and microscopy.[18] Currently, there are three commonly used methods to analyze and describe the polarization states: Jones vector analysis,[19] Stokes parameters,[20,21] and Poincaré sphere.[22,23] Conventional methods for detecting terahertz polarization typically entail the utilization of elements such

Y. Liu, Y. Xu, B. Yu, W. Liu, H. Cheng, S. Chen
The Key Laboratory of Weak Light Nonlinear Photonics
Ministry of Education
School of Physics and TEDA Institute of Applied Physics
Nankai University
Tianjin 300071, China
E-mail: wliu@nankai.edu.cn; hcheng@nankai.edu.cn; schen@nankai.edu.cn

The ORCID identification number(s) for the author(s) of this article can be found under https://doi.org/10.1002/apxr.202400100

DOI: 10.1002/apxr.202400100

Z. Zhang
School of Materials Science and Engineering
Chongqing Jiaotong University
Chongqing 400074, China

S. Chen
School of Materials Science and Engineering
Smart Sensing Interdisciplinary Science Center
Nankai University
Tianjin 300350, China

S. Chen
The Collaborative Innovation Center of Extreme Optics
Shanxi University
Taiyuan, Shanxi 030006, China

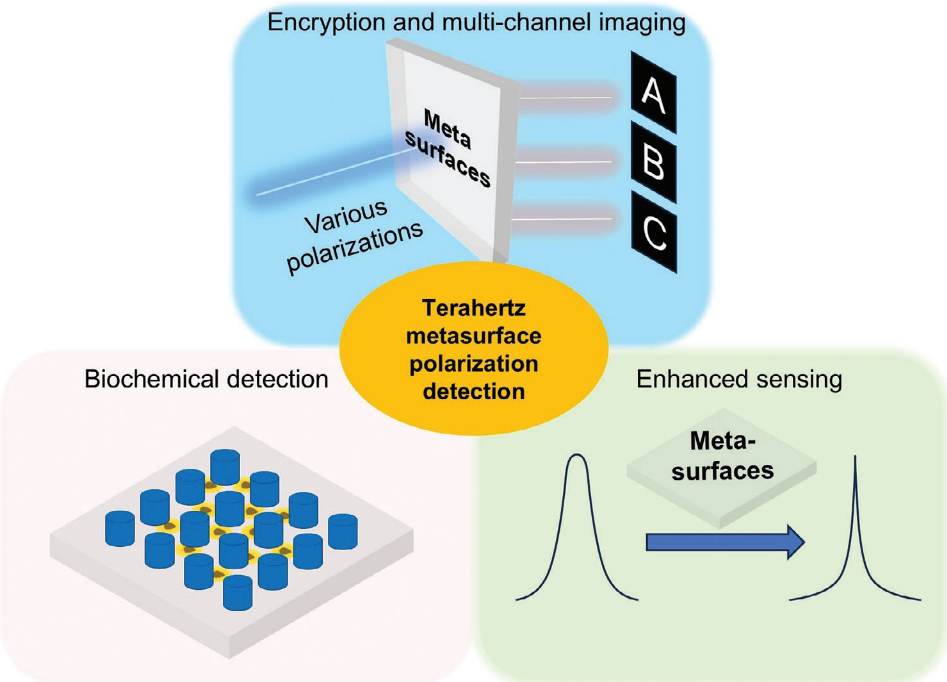

Figure 1. Terahertz metasurface polarization detection for different applications.

as polarizers, wave plates, or electro-optical crystals.[24–26] However, such elements and resulting optical systems are bulky and costly, hindering their widespread practical applications, miniaturization, and system integration. In recent years, metasurfaces have shown great potentials to solve these challenging problems. Metasurfaces are planar arrays of artificial microstructures supporting abundant EM resonances, and the dimensions of the unit cell are comparable or smaller compared with the operating EM wavelength. The modulation of EM waves is achieved by arranging meta-atoms in a predetermined order. The principle is to effectively control the EM wavefront by utilizing the abrupt phase changes of transmitted or reflected waves on the metasurface with the designed structure. This characteristic enables the manipulation of phase,[27–30] polarization,[31,32] amplitude,[33] and resonance frequency of waves.[34] Several effective designs with diverse functionalities have been demonstrated, such as the generation of specialized beams,[35–37] holography,[38,39] and metalenses.[40,41]

In this review, we focus on the recent development of terahertz metasurfaces in terms of polarization manipulation and detection. As shown in **Figure 1**, notable progress has been made in three primary applications, including image encryption, enhanced sensing, and biochemical detection. We introduce the fundamental principles of polarization, fundamentals of phase and polarization control and the description of polarization states, encompassing electric vector representation of polarized light, the Jones vector, the Stokes vector, and the Poincaré sphere. Then, we mainly introduce the research progress of terahertz metasurfaces in the aspect of polarization detection. Finally, we provide an overview of recent implementations of terahertz metasurfaces in the realm of polarization detection and offer insights into the challenges and prospects for future progress in this field.

2. The Description of Polarization States and Principles of Polarization Manipulation

As a fundamental property of light, polarization has been applied in various fields, such as optical displays, material characterization, and sensing.[42–44] Therefore, the precise characterization of polarization and its manipulation are two crucial goals. Traditional THz polarization controlling devices such as wave plates consider light's polarization as a homogeneous characteristic at the propagation cut-plane. Recently, advanced wavefront-shaping platforms called metasurfaces have been broadly developed, based on subwavelength arrays that can manipulate light's polarization point by point in space or time, thus expanding the scope of polarization optics and its applications. In this Section, we give a brief introduction to polarization theory, which is fundamentally required owing to the versatile capability of metasurfaces to control polarization. We then explore several mathematical representations of polarization states including Jones vector, Stokes parameters, and Poincaré Sphere, which provide powerful tools for adequate characterization of polarization states. Then, we discuss two principles of polarization manipulation that called Pancharatnam-Berry (PB) phase and electromagnetic multi-pole resonances, both have demonstrated strong capabilities to control the polarization state of light.

Light in free space is transverse EM waves, with the electric and magnetic fields oscillating in a plane perpendicular to the direction of propagation. Polarization pertains to the properties of light within this plane, and the trajectory of time varying electric fields defines the polarization state. The x and y components of the electric field along the z axis (direction of propagation) are given by

$$\boldsymbol{E}_x = E_x \cos\left(kz - \omega t + \delta_x\right) \tag{1}$$

$$\boldsymbol{E}_y = E_y \cos\left(kz - \omega t + \delta_y\right) \tag{2}$$

where E_x, E_y and δ_x, δ_y represent the amplitude and the phase at time instant t of light in the x, y directions, respectively. When eliminating the ωt term from the preceding equations, it can easily be shown that E_x and E_y satisfy the following equation:

$$\left(\frac{\boldsymbol{E}_x}{E_x}\right)^2 + \left(\frac{\boldsymbol{E}_y}{E_y}\right)^2 - 2\frac{\boldsymbol{E}_x}{E_x}\frac{\boldsymbol{E}_y}{E_y}\cos\delta = \sin^2\delta \tag{3}$$

where $\delta = \delta_x - \delta_y$ represents the relative phase difference between $\boldsymbol{E}_x$ and $\boldsymbol{E}_y$ components. Equation (3) represents an elliptical trajectory of the end of the electric field vector, where $\delta = 0$ or π indicates linear polarization state; $\delta = \pm\pi/2$, $E_x = E_y$ corresponds to a circular polarization state. Other cases represent the elliptical polarization states.

2.1. Jones Vector

When a monochromatic plane wave travels in free space along the z direction, the electric x and y components describe the polarization state since the E_z component is zero. In 1941, R. C. Jones introduced the concept of Jones vector:[45,46]

$$\begin{bmatrix} \boldsymbol{E}_x \\ \boldsymbol{E}_y \end{bmatrix} = \begin{bmatrix} E_x e^{i\delta_x} \\ E_y e^{i\delta_y} \end{bmatrix} \tag{4}$$

in which the $\boldsymbol{E}_x$ and $\boldsymbol{E}_y$ components share the same frequency and wavevector, allowing us to obtain complete polarization states regardless of specific time and positions. Jones vector represents the polarization state with the two orthogonal electric field amplitudes E_x and E_y, and the phases δ_x and δ_y. A concise form can be further written as:

$$\boldsymbol{E} = \begin{bmatrix} 1 \\ \frac{E_y}{E_x} e^{i\delta} \end{bmatrix} \tag{5}$$

A linearly polarized wave with amplitude E and a polarization angle θ relative to the x-axis can be represented by the normalized Jones vectors [cosθ sinθ]. For a circularly polarized wave with $E_x = E_y$ and $\delta = \pm\pi/2$, the Jones vector can be given by left-handed circularly polarized $\boldsymbol{E}_{LCP} = \frac{1}{\sqrt{2}}\begin{bmatrix} 1 \\ -i \end{bmatrix}$ and right-handed circularly polarized $\boldsymbol{E}_{RCP} = \frac{1}{\sqrt{2}}\begin{bmatrix} 1 \\ i \end{bmatrix}$.

In addition to its simple representation of the polarization state, the beauty of the Jones vector representation is that the effect of any homogeneous polarization device on a given polarization state can be obtained by multiplying the input Jones vector by a 2×2 matrix,

$$J = \begin{bmatrix} J_{11} & J_{12} \\ J_{21} & J_{22} \end{bmatrix} \tag{6}$$

where J_{11}, J_{12}, J_{21}, J_{22} represent the complex transmission coefficient of each component.[47] Therefore, if a given polarization state $\boldsymbol{E}$ passes through a polarized device whose Jones matrix is $\boldsymbol{J}$, the output polarization state $\boldsymbol{E}'$ can be expressed as $\boldsymbol{E}' = \boldsymbol{J}\boldsymbol{E}$. Accordingly, the output polarization state $\boldsymbol{E}'$ is $\boldsymbol{E}' = \boldsymbol{J}_n\boldsymbol{J}_{n\text{-}1}\ldots\boldsymbol{J}_1\boldsymbol{E}$ when light transmit through optical devices in a sequence with Jones vectors $\boldsymbol{J}_i$ (i = 1, 2, ..., n).

2.2. The Stokes Parameters and Poincaré Sphere

The Stokes parameters are more versatile to represent the polarization state of any EM waves, including completely polarized, unpolarized, or partially polarized waves.[48,49] This representation involves four handily measurable parameters that are specifically defined:

$$S = \begin{bmatrix} S_0 \\ S_1 \\ S_2 \\ S_3 \end{bmatrix} = \begin{bmatrix} I_0 \\ I_{\mathrm{H}} - I_{\mathrm{V}} \\ I_{+45^\circ} - I_{-45^\circ} \\ I_{\mathrm{RCP}} - I_{\mathrm{LCP}} \end{bmatrix} \tag{7}$$

where I_0 represents the intensity of the given light, and I_{H}, I_{V}, I_{+45°, I_{-45°, I_{RCP}, and I_{LCP} represent the intensity projected to the horizontal, vertical, +45°, −45°, right-handed, and left-handed bases, respectively. Equation (7) also provides an easy way to experimentally obtain the Stokes parameters by measuring the intensities of the given light in three orthogonal bases without phase measurement.

The Stokes parameters for a partially polarized light can be expressed as a sum of polarized and unpolarized components as $\boldsymbol{S}_{\mathrm{partially}} = \boldsymbol{S}_{\mathrm{polarized}} + \boldsymbol{S}_{\mathrm{unpolarized}}$, given by

$$\begin{bmatrix} S_0 \\ S_1 \\ S_2 \\ S_3 \end{bmatrix} = \begin{bmatrix} pS_0 \\ S_1 \\ S_2 \\ S_3 \end{bmatrix} + \begin{bmatrix} (1-p)\,S_0 \\ 0 \\ 0 \\ 0 \end{bmatrix} \tag{8}$$

The parameter p is the degree of polarization (DOP) of light, indicating the fraction of fully polarized light intensity.[50]

$$p = \frac{\sqrt{S_1^2 + S_2^2 + S_3^2}}{S_0} \tag{9}$$

Note that $p = 1$ represents the completely polarized light; $0 < p < 1$ represents partially polarized light; $p = 0$ represents unpolarized light, such as natural light.

For a completely polarized beam, the four Stokes parameters are not independent and the Stokes parameters can be given as:

$$\begin{cases} S_0 = I \\ S_1 = Ip\cos 2\chi \cos 2\psi \\ S_2 = Ip\cos 2\chi \sin 2\psi \\ S_3 = Ip\sin 2\chi \end{cases} \tag{10}$$

where ψ and χ represent the orientation and the ellipticity angle of the polarized electric component. The state of polarization of light can be described by a point on a sphere located at $(Ip, 2\psi, 2\chi)$ in the spherical coordinate. In the case of completely polarized

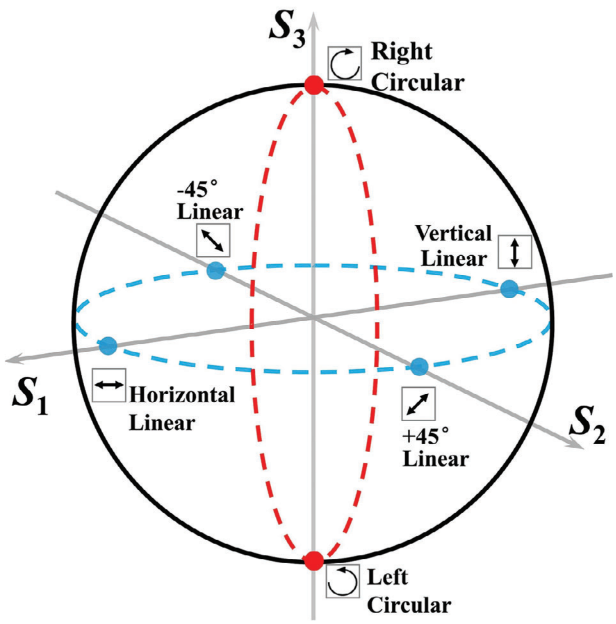

Figure 2. Representation of the Poincaré sphere and some common polarization states.

light, the mentioned sphere is called the Poincaré sphere, which was introduced by Henri Poincaré in 1892, as shown in **Figure 2**. Each point (S_1, S_2, S_3) on the sphere corresponds to a specific polarization state. The upper and lower vertices of the Poincare sphere correspond to the right-handed and left-handed circular polarization states, respectively. The points on the equator represent linearly polarized states with the polarization angle covering a range of 180°. The upper and lower hemispheres represent the right and left elliptically polarized light respectively. The ellipticity is nearly linear close to the equator, and approaches circular near the upper and lower vertices. This graphical representation significantly improves the simplicity to describe any polarization states, including their evolution in the parametric space.[51]

2.3. PB Phase

The PB phase originates from the transition between the local and laboratory coordinates, thus is independent of resonances of artificial structures.[52–54] For an anisotropic metasurface, the local coordinate u and v can be established along the fast and slow axes of the meta-atom. In general, the transmission process of metasurface can be written as:

$$J_\theta = \begin{bmatrix} t_u\cos^2\theta + t_v\sin^2\theta & \left(t_u - t_v\right)\sin\theta\cos\theta \\ \left(t_u - t_v\right)\sin\theta\cos\theta & t_u\sin^2\theta + t_v\cos^2\theta \end{bmatrix} \tag{11}$$

where t_u and t_v represent the transmission in the u and v directions, respectively. θ is the rotation angle of the meta-atom relative to the laboratory coordinate system. R(θ) is the rotation matrix. When the incident light is x-polarized, the transmitted or reflected light can be written as

$$\begin{bmatrix} E_x^{out} \\ E_y^{out} \end{bmatrix} = J_\theta \begin{bmatrix} 1 \\ 0 \end{bmatrix} = \begin{bmatrix} t_u\sin^2\theta + t_v\cos^2\theta \\ -\left(t_u - t_v\right)\sin\theta\cos\theta \end{bmatrix} \tag{12}$$

when the incident light is circularly polarized, the transmitted or reflected light can be written as

$$\begin{bmatrix} E_x^{out} \\ E_y^{out} \end{bmatrix} = \frac{J_\theta}{\sqrt{2}} \begin{bmatrix} 1 \\ i\sigma \end{bmatrix} = \frac{1}{2\sqrt{2}} \left(\left(t_u + t_v\right) \begin{bmatrix} 1 \\ i\sigma \end{bmatrix} + \left(t_u - t_v\right) e^{2i\sigma\theta} \begin{bmatrix} 1 \\ -i\sigma \end{bmatrix} \right) \tag{13}$$

where $\sigma = \pm 1$ represent the right-handed and left-handed circular polarization states, respectively. The first term on the right side in the equation shows the co-polarization, while the second term represents the cross-polarization state with an additional PB phase of $2\sigma\theta$. The phase is related to the rotation angle of the subwavelength meta-atom. PB metasurfaces have significantly expanded our controllability on polarized light, stimulating many fascinating applications such as efficient polarization detectors and meta-holograms.

2.4. The Electric Dipole Resonance and Magnetic Dipole Resonance

The resonance of subwavelength unit cell with incident light fields at specific frequency allows for the functionalization of metasurfaces, such as local field enhancement and polarization conversion. The field distribution coherently enhanced by the designed artificial structure is called the resonance mode. These resonances indicate the interaction mechanism between light and metasurfaces, enabling accurate manipulation of the polarization state of light. Metasurfaces can support various local resonance modes such as electric dipole, magnetic dipole, electric quadrupole, magnetic quadrupole resonance and so on.[55,56]

An electric dipole is effectively formed by two point charges $+q$ and $-q$ connected by a vector $\boldsymbol{p}$ known as an electric dipole moment $|\boldsymbol{p}| = qd$, where q is the absolute value of one of the two charges and d is the distance between the two charges. The direction of the dipole moment starts from the negative charge to the positive charge. The electric dipole resonance serving as a time-varying current can also be excited by EM waves interacting with rectangular metallic or dielectric structures. With an external electric field, the effective positive charges are forced to one side of the metallic rod, while negative charges are forced to the opposite one. The magnetic dipole, equivalent to a flow of electric charge around a loop, includes such as the electrons circulating around atomic nuclei, electrons spinning on their axes, or rotating positively charged atomic nuclei. The magnetic dipole moment of a current loop carrying current I with area A is defined as $|\boldsymbol{m}| = IA$, and the direction of the magnetic dipole moment is perpendicular to the plane of the current loop. By using metallic split-ring resonators,[57] where the conduction current loop within the split-ring resonators that is driven by incident fields can lead to the formation of an effective magnetic dipole. The multipole resonances, can be regarded as the higher-order term of the dipole mode. In general, the contribution of the higher-order resonances can be evaluated using perturbation theory, for some specific structures or materials, the impact of higher-order terms on the radiation field could be significant.

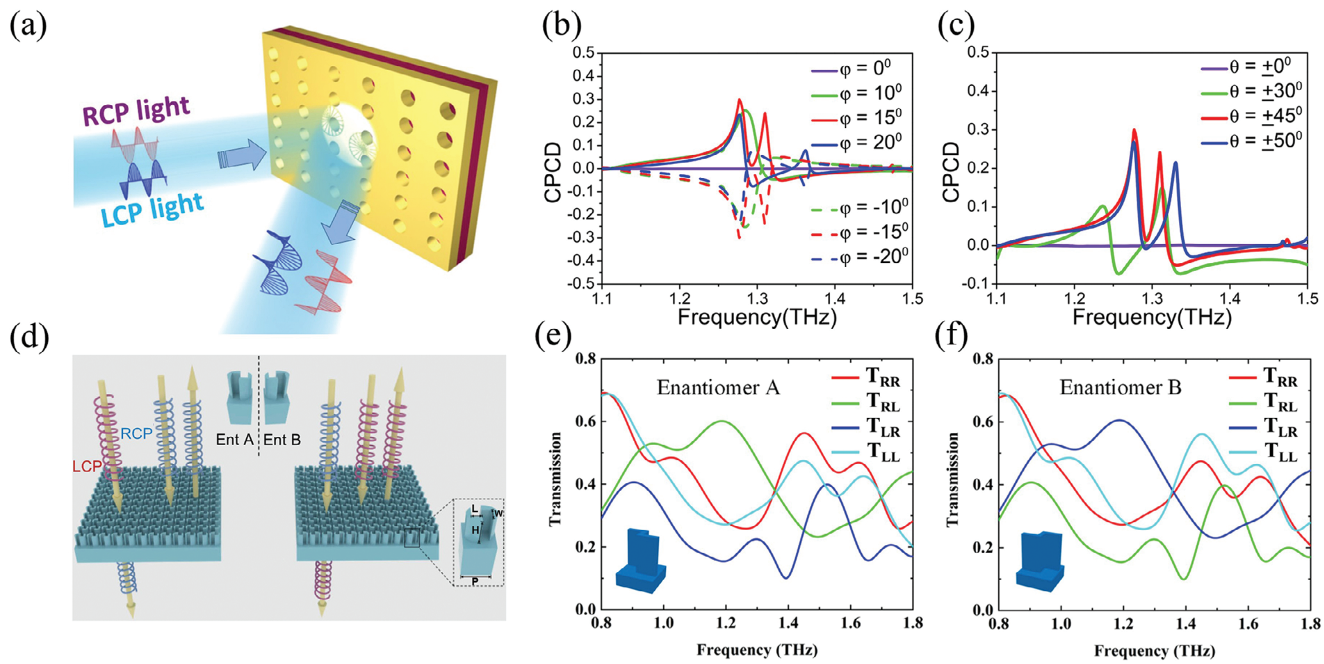

Figure 3. Polarization conversion based on artificial structures. a) Terahertz metasurface with dual-band strong extrinsic 2D chirality. b,c) The circular polarization conversion difference tuned by incident angles. a–c) Reproduced with permission.[58] Copyright 2016, OSA. d) Meta-atom enantiomers with contrasting chiralities. Reproduced with permission.[61] Copyright 2021, OSA. The transmission of e) Enantiomer A and f) Enantiomer B for contrasting chiralities. e,f) Reproduced with permission.[62] Copyright 2021, AIP Publishing.

3. Spatially-Uniform Polarization Manipulation and Detection

In general, the artificial sub-wavelength structures like metasurfaces have provided excellent platforms for polarization manipulation in the terahertz band. For example, Cao et al. theoretically demonstrated a terahertz metasurface with a dual-band strong extrinsic chirality originating from the incline incidence, as shown in **Figure** 3a. Figure 3b,c demonstrate that the achiral metasurfaces with a large circular polarization conversion difference can be tuned by the incident angle, which can be applied for chiral sensing and highly efficient polarization conversion.[58] The intrinsic chirality for polarization conversion can be achieved by breaking the structural symmetry along the direction of incidence. Yin et al. observed the asymmetrically and circularly cross-polarized transmission from the circular cross-polarization conversion spectra and the circular conversion dichroism of the chiral metasurfaces.[59] Ma et al. proposed a novel all-dielectric metasurface exhibiting quasi-bound states in continuum with a high Q factor and strong circular dichroism for both transmitted and reflected waves by simultaneously breaking the in-plane and mirror symmetries. The metasurface with high Q factors and strong circular dichroism paves a new way for practical applications, such as chiral sensing.[60] Combining structures with various chiralities can achieve more complex functions. As shown in Figure 3d, Li et al. proposed a pair of lossless all-silicon metasurfaces achieving giant intrinsic chiralities in the terahertz band. The spin-dependent and tunable near-field image is displayed by arranging the two kinds of meta-atom enantiomers.[61] Similarly, Zheng et al. proposed a pair of all-silicon metasurfaces with contrasting chiralities to achieve highly efficient circular polarization differential transmittance in the terahertz band. Specifically, the circularly polarized transmission coefficients of Enantiomer A are depicted in Figure 3e, and that of Enantiomer B are depicted in Figure 3f.[62] In addition, Yang et al. proposed a dual-frequency structure consisting of a quarter-wave plate, a polyimide spacer, and a filter, to distinguish the handedness of circularly polarized light by filtering. The extinction ratio is 4 dB at 0.952 THz and 5.26 dB at 1.03 THz, and the maximum transmittance efficiency reaches 40%.[63]

Furthermore, the pump methods based on light, thermo, electricity, and magneto have been presented to realize dynamic polarization manipulation and detection. By applying an external pump to phase-change materials such as vanadium dioxide, the properties of the materials can be changed, so that the inherently chiral metamaterial structures can achieve dynamic polarization conversion. For example, a chirality-tunable terahertz metasurface for dynamic polarization conversion was proposed by Yang et al., based on a 3D folded structure with vanadium dioxide. By folding the split ring resonators at a certain angle, the mirror symmetry of the structure is broken. Additionally, the dynamic tuning of circular dichroism effect can be realized by adjusting the conductivity of VO_2 by pump. When VO_2 is gradually changed from an insulating state to a metallic state with the increase of conductivity, the metasurface could be switched between the "ON" and "OFF" modes of chiralities.[64] As shown in **Figure** 4a, Kobachi et al. proposed a dynamic reflective metasurface based on a phase transition of vanadium dioxide that induces the necessary structural transformation of the metallic patterns. Figure 4b depicts that the dynamic helicity inversion is at 0.90 THz with a conversion efficiency of over 80%.[65] Lv et al. investigated the versatile polarization manipulation in a

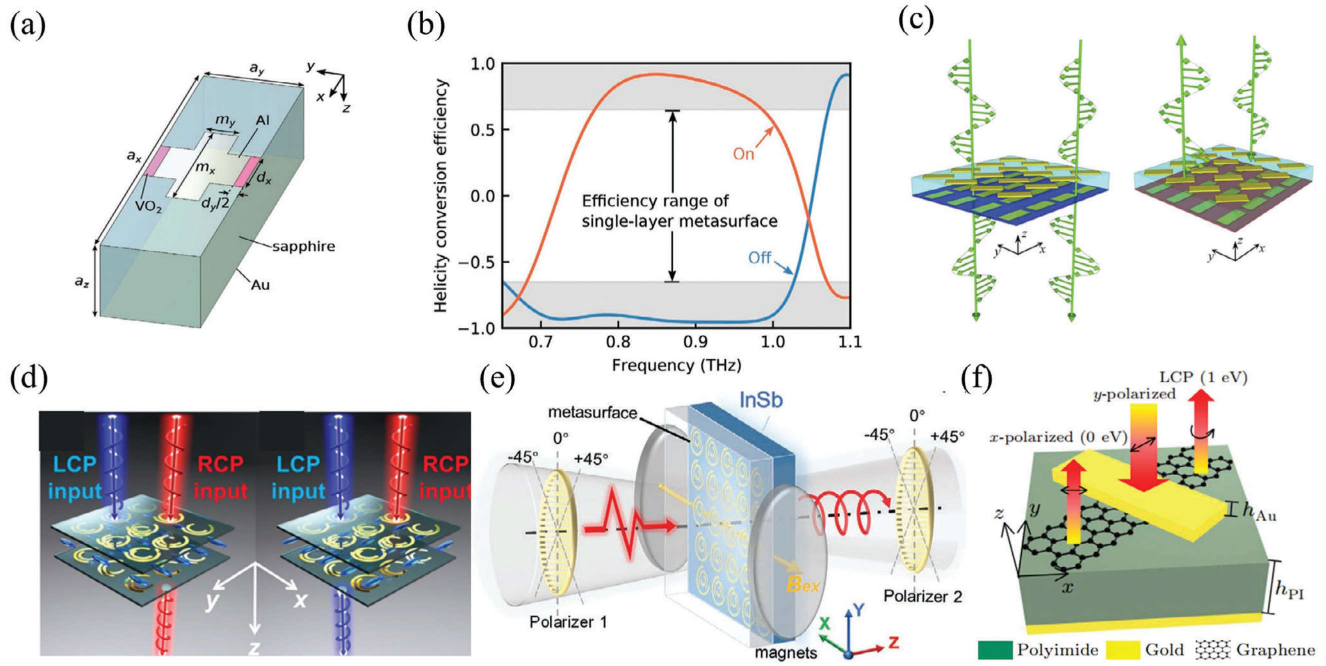

Figure 4. Polarization conversion based on pump manipulation. a) Reflective terahertz metasurface based on the phase-change of vanadium dioxide with b) switchable helicity conversion efficiency a,b) Reproduced with permission.[65] Copyright 2021, John Wiley and Sons. c) Vanadium dioxide terahertz metamaterials for versatile polarization manipulation. Reproduced with permission.[66] Copyright 2022, OSA. d) Dual-layer tunable terahertz chiral device. Reproduced with permission.[67] Copyright 2023, OSA. e) Dynamic polarization conversion based on hybrid magneto-optical metasurface. Reproduced with permission.[68] Copyright 2021, John Wiley and Sons. f) Broadband switchable chiral metasurface consisting of polyimide, gold, and graphene. Reproduced with permission.[69] Copyright 2023, IOP Publishing.

vanadium dioxide terahertz metamaterial, as shown in Figure 4c. The phase change of vanadium dioxide enables flexible switching between dual-band asymmetric transmission and dual-band reflective half-wave plate. This switchable polarization metamaterial could advance multichannel polarization detection.[66]

Apart from vanadium dioxide, materials such as graphene, liquid crystals, and InSb can also achieve dynamic polarization conversion. As shown in Figure 4d, Jiang et al. demonstrated a dynamic terahertz chiral device based on a composite structure of anisotropic liquid crystals sandwiched between a bilayer metasurface. The device supports symmetric and antisymmetric modes under the incidence of left-circularly and right-circularly polarized waves, respectively. The varying coupling strength of the two modes responds the chiralities of the device. Due to the anisotropy of the liquid crystals, changing the coupling strength of the modes can bring tunability to the chiral device.[67] Fan et al. designed a scheme for dynamic terahertz anisotropy and chirality manipulations based on the hybrid magneto-optical metasurface with transversely magnetized InSb. The study revealed a special transverse photonic spin state in the InSb and a transverse-longitudinal spin coupling effect in the hybrid magneto-optical metasurface in Figure 4e. This hybrid magneto-optical metasurface achieves a polarization conversion rate of near 100% and an induced intrinsic chirality of over 15 dB, leading to some intriguing applications like polarization imaging, chiral spectroscopy, and chiral sensing.[68] As shown in Figure 4f, Luo et al. achieved the broadband switchable device in the terahertz band, by varying the graphene Fermi energy of a graphene-metal metasurface. The reflective metasurface can be switched between the function of half-wave plate with polarization conversion ratio exceeding 0.97 over a wide band ranging from 0.7 to 1.3 THz, and the function of quarter-wave plate with ellipticity above 0.92 over 0.78 THz – 1.33 THz. The shared bandwidth reaches up to 0.52 THz with a relative bandwidth as high as 50%.[69]

In addition, exceptional points (EPs) are singularities of non-Hermitian Hamiltonians used to characterize systems with open boundaries enabling energy exchange with environment or material gain or loss. These points are sensitive to perturbations in the system and can be utilized for polarization detection. For example, Li et al. took graphene as an alternative to metal for antennas to investigate EPs in polarization space. They demonstrated that EPs always emerge in pairs within the terahertz band by tuning the geometric parameters and incident wavelengths. As a result, the chirality of two EPs is completely opposite related to left circular polarization or right circular polarization output, and could be altered by adjusting the incident direction and displacements of two graphene strips along horizontal and vertical directions.[70] Another example involved adjusting the external voltage to tune the Fermi level of the Dirac semimetal, enabling the transitioning from the PT symmetry phase to the PT symmetry-breaking phase. Yang et al. designed a tunable metasurface with bulk Dirac semimetal for dynamic polarization manipulation, which could be applied for polarization detection, manipulation, and ultrasensitive sensing.[71]

Moreover, metasurfaces could exhibit polarization-selective absorption for incident terahertz waves with different polarization states due to the broken symmetry in the x-direction and y-direction of planar structure. Hu et al. fabricated

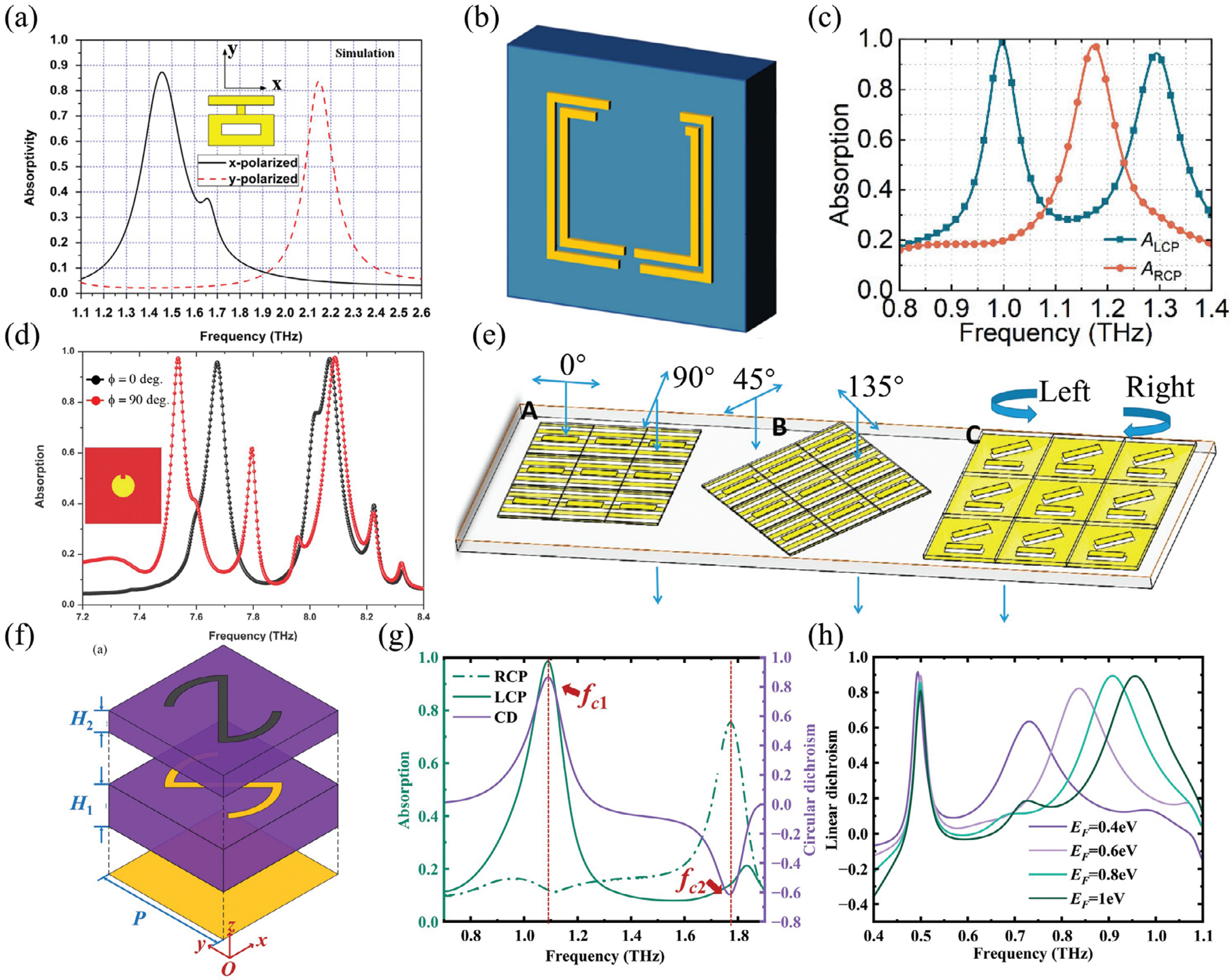

Figure 5. Polarization-selective absorption. a) Structure and spectra of terahertz metamaterial absorber with polarization dependence. Reproduced with permission.[72] Copyright 2014, Elsevier. b) Terahertz chiral metasurface with c) polarization-selective absorption. b,c) Reproduced with permission.[73] Copyright 2022, The Authors, published by MDPI. d) Circular metallic structure without a square and dual-band absorption based on polarization angles. Reproduced with permission.[74] Copyright 2024, John Wiley and Sons. e) Polarization-dependent transmission and absorption metasurfaces. Reproduced with permission.[75] Copyright 2023, MDPI. f) Terahertz dichroic device with g) circular dichroism and h) tunable linear dichroism. f–h) Reproduced with permission.[76] Copyright 2023, Elsevier.

a polarization-dependent terahertz metamaterial absorber, as shown in **Figure 5a**. The absorptivity for x-polarized wave is ≈0.9 at 1.42 THz, and for y-polarized wave is ≈0.87 at 2.15 THz. It has potential applications based on the metamaterial absorber, such as terahertz polarization imaging, sensing, and detection.[72] As shown in Figure 5b, Zhang et al. proposed a triple-band terahertz chiral metasurface. Figure 5c illustrates the absorption for left circular polarization or right circular polarization in three distinct frequency bands.[73] Teber designed a dual-band terahertz absorber metasurface structure, which consists of a metallic base plane, a dielectric layer on this plane, and a circular metallic without a square. Figure 5d demonstrates the absorption spectra of the metasurface structure based on the polarization angle.[74] Yang et al. proposed polarization-dependent metasurfaces in Figure 5e, which allows two types of polarization information to be obtained simultaneously in a single beam of light. Meanwhile, the circular polarization-dependent structure has a transmission extinction ratio of 8.1 dB and an absorption extinction ratio of 4.66 dB at 2.8 THz.[75] Furthermore, Chen et al. proposed a terahertz dichroic device based on a patterned graphene layer and a gold layer, as shown in Figure 5f. Figure 5g depicts that the proposed device can achieve maximum circular dichroism values of 0.866 at 1.09 THz and −0.614 at 1.76 THz, and maximum linear dichroism values of 0.779 at 0.51 THz and −0.633 at 0.76 THz. The dichroism of the device can be controlled through multiple dimensions, such as the Fermi level of graphene, as shown in Figure 5h.[76] These works of polarization-selective absorption are beneficial for the development of high-resolution terahertz polarization imaging and detection.

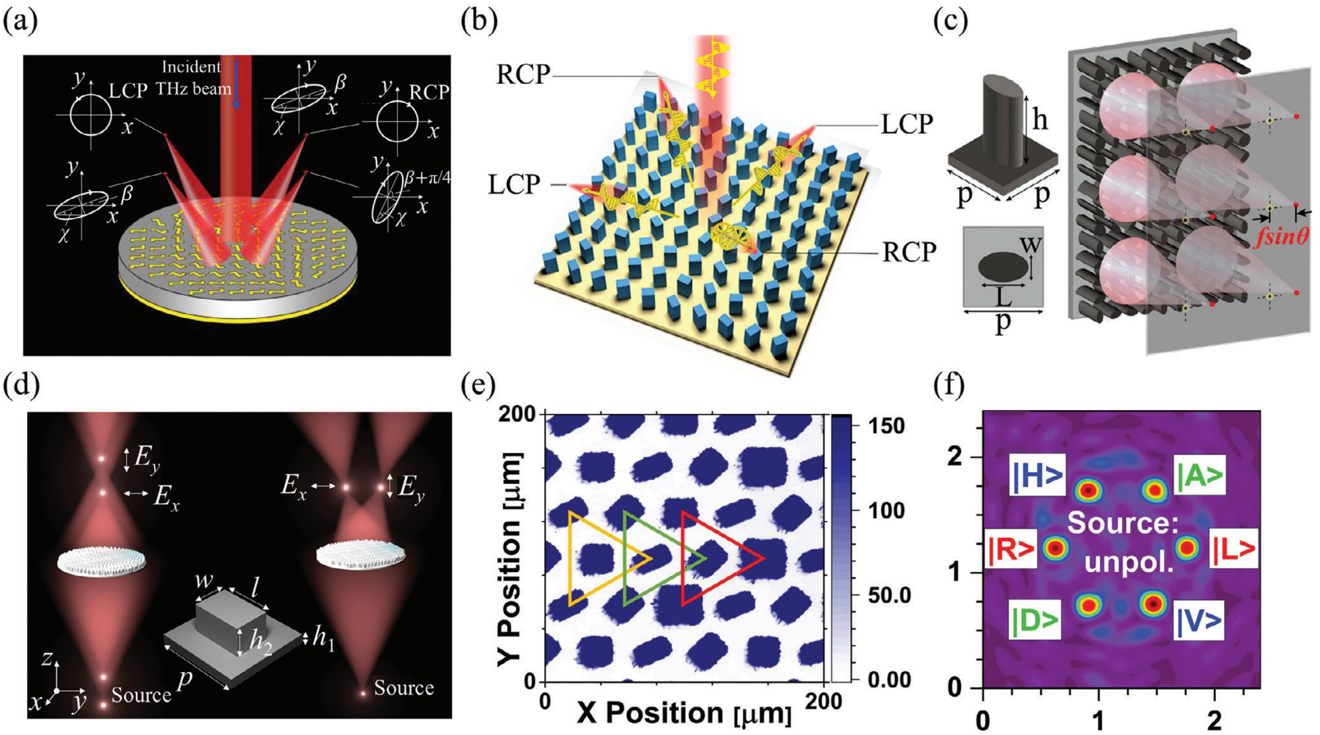

Figure 6. Polarization-selective focusing. a) Reflective terahertz metalens with four focal points. Reproduced with permission.[77] Copyright 2020, OSA. b) Multifocal metalens with four focal points. Reproduced with permission.[78] Copyright 2024, Elsevier. c) Polarimeter for detecting the incident angle and polarization state of incident light. Reproduced with permission.[79] Copyright 2020, John Wiley and Sons. d) Metalens with two orthogonally polarized point sources. Reproduced with permission.[80] Copyright 2021, MDPI. e) The three sub-lattices structure of metasurface polarimeter f) to focus terahertz waves into six focal points polarization-selectively. e,f) Reproduced with permission.[81] Copyright 2022, OSA.

4. Spatially-Distributed Polarization-Selective Manipulation and Detection

Compared with the methods of spatially-uniform polarization, the spatially-distributed polarization-selective methods can also achieve manipulation and detection of polarization. For example, the polarization-selective focusing method based on the PB phase can be utilized to selectively focus incident waves on specific focal points according to their polarization states. The encoding technique with a decoupling effect imparts phase profiles with off-axis bifocal characteristics to various polarization states, respectively. By extracting the complex amplitude information at different positions on the pixelated focal plane, the key parameters of the full Stokes matrix as well as the polarization states can be reconstructed continuously. As shown in **Figure** 6a, Wang et al. proposed a reflective terahertz metalens for polarization detection with four focal points. The polarization states include left circular polarization, right circular polarization, and two kinds of elliptical polarization. By measuring the intensities of four focal points, the handedness, ellipticity, and major axis of the polarization state can be determined. This capability is attractive for applications in terahertz polarization detection.[77] With a similar design of reflective metalens with four focal points, Jiang et al. demonstrated multifocal metalens controlled by circular polarization multiplexing, as shown in Figure 6b. Under normal incidence of linearly polarized light, a metalens generates two points for left-circularly polarized light conversion and two points for right-circularly polarized light conversion.[78] As for transmissive metalens, Zhang et al. demonstrated a new type of polarimeter for detecting the incident angle and polarization state of incident light simultaneously, as shown in Figure 6c. The polarimeter with 2×3 subarrays can control the polarization and phase of light and achieve polarization detection using modified Stokes parameters.[79] Moreover, Zhou et al. proposed the terahertz spherical aberration-corrected metalens to achieve polarization-multiplexed imaging. Figure 6d depicts the schematic of the spherical aberration-corrected metalens, where two orthogonal polarization point sources are imaged at different longitudinal and transverse positions. This work for terahertz polarization imaging introduces a novel approach to achieving multifunctional beam steering, tomographic imaging, and chiroptical detection.[80] Nowack et al. designed a metasurface polarimeter with three triangular sub-lattices in Figure 6e to focus terahertz waves into six focal points polarization-selectively, as shown in Figure 6f. The maximum average measurement accuracy of multiple measurements is 92.1%.[81]

In addition, Li et al. demonstrated a new scheme for efficiently realizing miniaturized polarization detection based on the polarization multiplexing encoding technique. The full Stokes parameter matrix of the incident polarization state can be reconstructed in a single snapshot by recording the complex amplitude information contained in a pre-designed plane. This work offers a potential photonic meta-platform for polarization detection.[82] Zhang et al. directly applied the concept of phase discontinuities to surface wave launching with metasurfaces, which is sensitive to both the incident polarization and the surface wave dispersion. The polarization state could be decoded by extracting the amplitude and phase information of the surface waves in both directions representing the left circular polarization and the left circular polarization components. This property of polarization-switchable wavefront shaping could realize the functions of polarization detection and sensing.[83] Therefore, by using metalenses and other artificial structures to focus polarized terahertz waves onto different points of the focal plane, it is possible to extract complex amplitude information at various points and reconstruct the parameters of the full Stokes matrix. These spatially polarization-selective methods can obtain the full Stokes polarization parameters and the specific polarization states of the incident terahertz wave. It is significant for terahertz polarization manipulation and detection, which can be applied in polarization imaging, chiral sensing, and non-destructive evaluation in terahertz band.

Another spatially-distributed polarization-selective scheme for polarization manipulation and detection relies on the generating vortex beams through metasurfaces. It is based on the independent control of left-handed and right-handed circularly polarized terahertz waves. Through the modal analysis of the transmitted fields modulated by metasurfaces, the parameters describing the incident polarization states could be obtained. Subsequently, the incident polarization states could be reconstructed using the full-Stokes parameters. For example, Min et al. proposed a notched concave metasurface to generate multifunctional vortex beams like four vortex beams, focusing vortex beams, deviation focusing vortex beams, and multi-beam vortex beams. Each vortex beam corresponds to various polarization states.[84] As shown in **Figure 7a**, Jiang et al. proposed a metallic waveguide array to determine the polarization state by measuring both the phase difference and amplitude ratio of its two orthogonal components, which is based on the generation and interference of polarization-multiplexing vortex beams. When a fully polarized terahertz wave passes through the waveguide array, its two orthogonal components will be converted into $+1^{st}$- and -1^{st}-order Bessel vortex beams. The phase difference and amplitude ratio of these beams are related to the polarization state of the incident waves.[85] Xu et al. proposed all-silicon quasi-periodic arrays based on polarization multiplexing technology, which can be used for detecting arbitrary incident linear polarization states. By embedding independent helical phase profiles in two orthogonal linear polarization channels, the generated interference spot at the pre-designed focal plane is resolvable to determine the incident polarization state in the polarized direction.[86] As shown in Figure 7b, Zheng et al. demonstrated a terahertz polarization detection scheme by using the reconstructed complete polarization parameters of the transmitted vortex field. The detected polarization states of linear polarizations, circular polarizations, and elliptical polarization are characterized by polarization ellipses, Poincaré sphere, and full Stokes parameters.[87] Then they established a connection between the generated longitudinally polarized vortex and the polarization parameters of the incident field by finely designing a phase profile of the all-silicon metasurface. The polarization detection based on the mode analysis of transmitted longitudinally polarized vortex field is depicted in Figure 7c.[88]

Therefore, the polarization detection based on vector beams provides a potential platform to determine the polarization state of terahertz waves. It is significant for accelerating the practical applications of terahertz waves in polarization detection, multiplexing communication, and chiral sensing. Li et al. achieved the reconstruction of the full Stokes parameter matrix in the terahertz band by establishing an all-silicon decoupled metasurface based on the polarization multiplexing encoding technique. Figure 7d illustrates the working principle of the decoupled metasurface with central focusing characteristics. This scheme offers opportunities for ultra-compact, high-resolution full-Stokes polarization imaging.[89] Moreover, combining off-axis dual-focus and vector vortex beams, Tian et al. proposed a novel method to provide potential solutions for miniaturized polarization detection. The ellipticity and handedness of incident terahertz waves can be determined by the electric field intensity ratio of the two off-axis focused spots. Additionally, the major axis direction of linear polarization waves can be determined by extracting the azimuth of the vector vortex beams.[90] In order to realize the tunable polarization conversion, Li et al. constructed a terahertz rotated metalens, as shown in Figure 7e. By rotating the metalens at a certain angle to control the conversion of multi-polarization states, the incident linear polarized terahertz waves can be converted to three polarization states, i.e., linear polarization without conversion, LCP and RCP. This multi-functional metalens is expected to be used in the advanced terahertz camera for polarization imaging.[91] In summary, the polarization-selective focus and constructing vector beam offer effective methods to achieve the spatially polarization-selective manipulation and detection for terahertz waves.

5. Applications

5.1. Enhanced Sensing by Terahertz Polarizer

As mentioned previously, metasurfaces have demonstrated a significant localized resonance and field enhancement, leading to a notable improvement in sensing capabilities. The effectiveness of localized resonance sensing primarily hinges on monitoring changes in intensity spectrum and frequency shift of the resonance peak within the THz spectra. Recent studies have investigated THz chiral sensing enhanced by metasurfaces, utilizing the polarization conversion and selection properties of chiral metasurfaces.[92–94] Polarization sensing exhibits higher quality (Q) factor and figure of merit (FoM) compared with conventional THz transmission resonance sensing.[95] This approach could obtain richer sensing information and better sensitivity, and has been widely used in the field of THz sensing.

For example, Liu et al. employed a polarization-dependent metasurface to investigate the inhibition effects of aspirin on cell proliferation through THz polarization sensing,[96] as shown in **Figure 8a,b**. The study presented a significant enhancement in the Q factor and FoM of polarization sensing, which are 4 to 5 times higher than that in traditional resonant sensing. The minimum cell concentration obtained by resonance sensing was 5.88×10^4 cells mL^{-1}, while polarization sensing achieved comparable results with a substantially reduced concentration of 3.0×10^3 cells mL^{-1}. This observation shows the promising

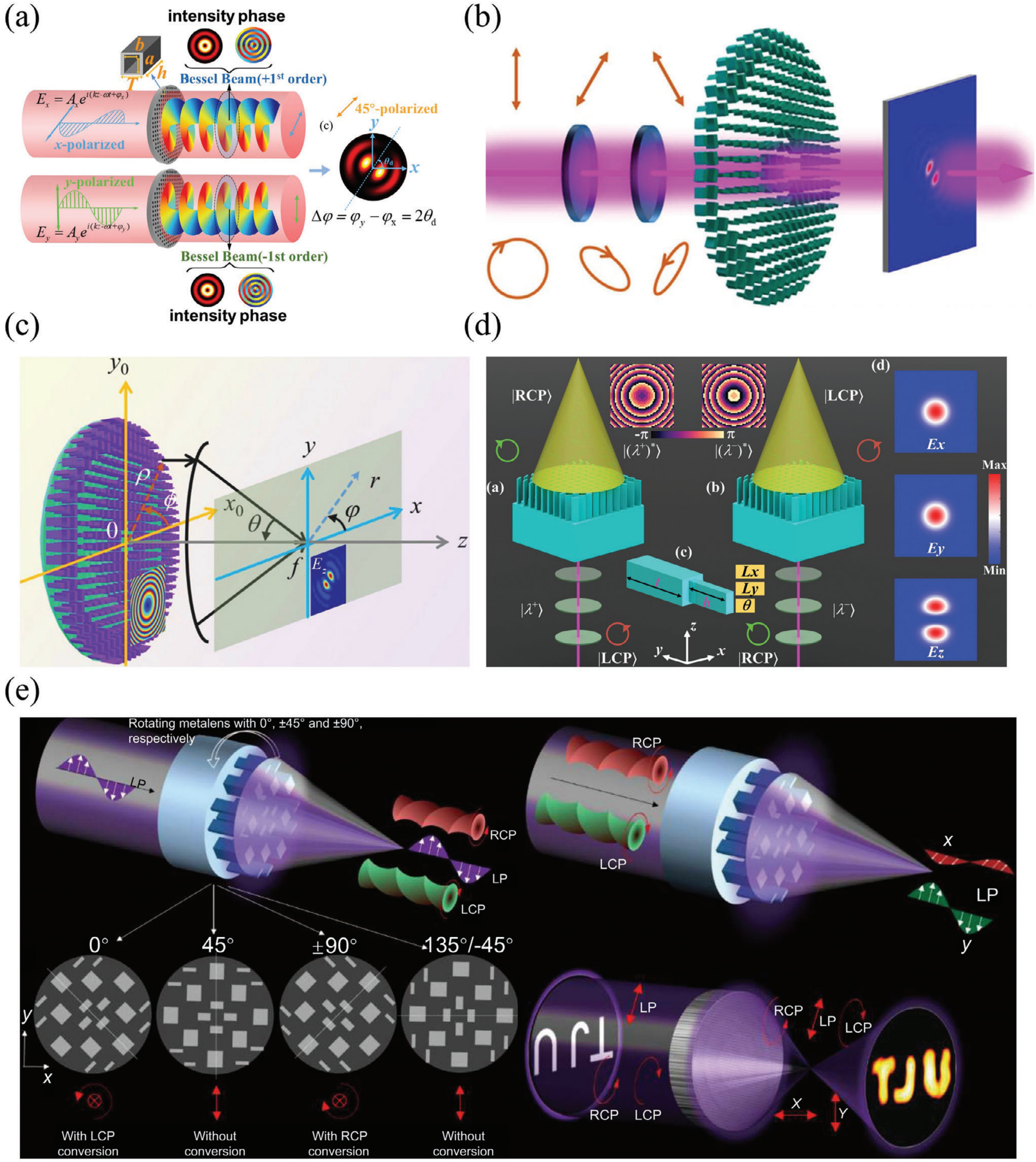

Figure 7. Constructing vector beam. a) A schematic for determining the polarization state based on metallic waveguide arrays. Reproduced with permission.[85] Copyright 2023, John Wiley and Sons. b) A terahertz polarization-parameters reconstruction scheme by transmitted vortex field. Reproduced with permission.[87] Copyright 2023, OSA. c) A metasurface for mode analysis of transmitted longitudinally polarized vortex fields. Reproduced with permission.[88] Copyright 2024, Elsevier. d) A central focusing scheme to construct vector beams based on the decoupled metasurface. Reproduced with permission.[89] Copyright 2023, John Wiley and Sons. e) Terahertz rotated tunable metalens for multifunctional polarization conversion and focusing. Reproduced with permission.[91] Copyright 2022, Opto-Electronic Advances.

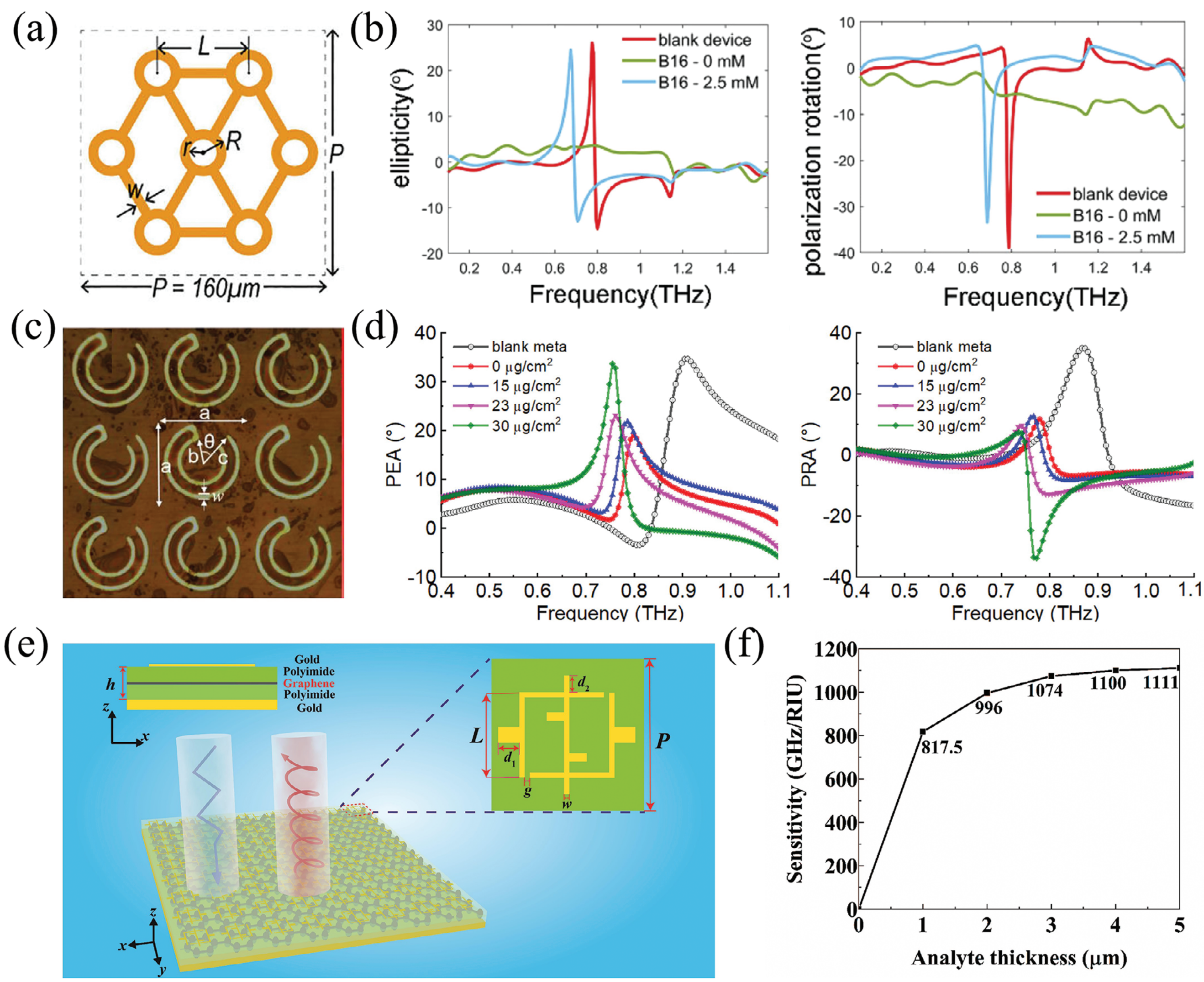

Figure 8. Polarization-enhanced sensing. a,b) Measurement of cell proliferation under aspirin inhibition with a) the geometric structure of unit cell of the metasurface and b) transmissive wave polarization information of B16 including polarization ellipticity spectra (left) and polarization rotation angle spectra (right). a,b) Reproduced with permission.[96] Copyright 2020, OSA. c,d) Quantitative detection between different lactose concentrations with c) the micrograph of the flexible metasurface sensor and d) experimental polarization ellipticity (PEA) and the polarization rotation angle (PRA) of THz flexible metasurface sensing attached with lactose-polyvinyl alcohol films of different concentrations. c,d) Reproduced with permission.[97] Copyright 2022, Elsevier. e,f) Hybrid resonator-graphene metasurface with a refractive index distinguish sensitivity can reach 1074 GHz/RIU. e) The schematic view and the geometric dimensions of the meta-atom as well as the detailed layered structures and f) the relationship between analyte thickness and sensitivity. e,f) Reproduced with permission.[98] Copyright 2023, OSA.

potential of THz polarization sensing in biological investigations. However, THz polarization sensing faces challenges related to strong absorption, particularly in aqueous solutions. Zhong et al. proposed an ultra-thin flexible metasurface sensor via THz polarization sensing,[97] as shown in Figure 8c. The metasurface localized and enhanced THz waves and exhibited minimal absorption due to its extremely thin profile, which improved the sensing sensitivity. Figure 8d illustrates the polarization ellipticity (PEA) and the polarization rotation angle (PRA) of the output light corresponding to varying concentrations of lactose. Compared with the blank metasurface, the shape of the lines changed regularly with the increase of lactose concentration, which is different from the resonant sensing. The study indicates that minute quantities of lactose as low as 35 μg on the metasurface can be detected, with a sensitivity reaching 1.43 GHz/(μg cm^{-2}) or 0.57°/(μg cm^{-2}), surpassing the sensitivity of resonance sensors by 1.5 times. Graphene metasurfaces have demonstrated significant effectiveness in generating localized resonance and field enhancement. Hao et al. proposed a precise refractive index sensing capabilities achieved through dynamically modulated Fano resonances of circularly polarized waves utilizing a hybrid resonator-graphene metasurface,[98] as shown in Figure 8e. By adjusting the Fermi level of graphene, the metasurface successfully achieved high-precision detection across a refractive index range of 1-1.6. Furthermore, Figure 8f represents that a refractive index distinguish capability of

1/10 000 can be attained with the polarization extinction ratio below −50 dB, while the sensitivity could reach 1074 GHz/RIU.

5.2. Biochemical Substances with THz Polarization Detection

The THz polarization sensing techniques and metamaterial sensors have emerged as a potential approach to THz biochemical sensing, offering better sensitivity, accuracy, and comprehensive insights into the anisotropy and chirality of samples. For example, the circular polarization spectra of chiral isomers display distinct fingerprint features that are specific to each isomer. Through the analysis of the circular polarization spectrum of a chiral isomer, researchers can obtain precise details regarding its chemical composition and distinguish it from other isomers.[99] In addition to chiral isomer identification, THz polarization sensing methods have been employed in diverse fields such as physicochemical processes of a protein, cell biology, and virus detection. These methods present significant benefits in various fields of biochemical sensing.[100]

Amin et al. presented a technique to distinguish three viruses that possess comparable optical properties by employing a graphene plasmonic metasurface combined with polarization sensing.[101] The chiral unit cell with a split-ring configuration is adopted which consists of two L-shaped graphene elements of slightly different dimensions, as shown in **Figure 9a**. The graphene-based plasmonic metasurface constructed with chiral unit cells exhibits significant near-field enhancement, thus inducing a sharp variation in the phase discrepancy between the electric field vector components. This results in a swift transition of the reflected THz polarization states from left-handed to right-handed ones. The polarization states of three different strains of influenza viruses H1N1, H5N2, and H9N2 are shown at two resonant frequencies 1.364 and 1.717 THz in Figure 9b. Each virus can be uniquely traced by linearly polarized, left-handed or right-handed elliptically polarized reflection. In 2021, Chang's group introduced a new THz sensing method based on THz reflective time-domain polarization spectroscopy (RTDPS) system and a chiral metasurface sensor.[102] Figure 9c shows the structure parameters and the micrograph of the fabricated metasurface, the single-layer spiral metasurface can exhibit strong chirality, leading to the strong capabilities of polarization conversion and chiral selectivity for THz waves. As shown in Figure 9d, the structural formulas of D- and L-proline are similar. However, it can be seen from the ellipses that the output polarization states of D- and L-proline, especially in the polarization rotating angle, have a great difference at the same concentration and frequency.

In another work, they developed a versatile twisted dual-layer metasurface sensor to identify protein concentrations.[103] The peak value and difference of the circularly polarized spectrum as the denaturation degree of the bovine serum albumin (BSA), the whey protein (WP), and the ovalbumin (OVA) protein solutions increase from 0% to 100%. The circularly polarized spectra of the three proteins exhibit distinct characteristics during thermal denaturation due to their unique molecular structures. Moreover, Shi et al. proposed a THz phase shift sensing method based on a polarization-dependent electromagnetically induced transparency (EIT) metasurface, which was performed for amino acid enantiomers detection.[104] Figure 9e shows the schematic of the metasurface consisting of double-ring arrays. Based on the isoelectric point theory, an amino acid will carry a positive charge when its isoelectric point exceeds the pH of the solvent. In the case of Arg, with an isoelectric point of 10.7, it is positively charged and is different from other amino acids such as Pro, Cys, and Ala. Therefore, Arg is uniquely capable of attaching to the functionalized metasurface via electrostatic adsorption, and Figure 9f reveals that the frequency shift for Arg at concentrations of 10 and 40 mg ml^{-1} are both highest compared with Cys, Ala and Pro, allowing for the distinction between Arg and the other three amino acids. For Lactic acid (LA) detection, Yang et al. reported a method for the identification of chiral LA enantiomers (D-LA and L-LA).[105] This method employs an achiral THz EIT metasurface to measure the chiral enantiomers present in LA samples. The chiral parameters can be extracted from the circular polarization transmission coefficients. Notably, the sensor spectra of LAs with different chirality exhibit a consistent redshift as the concentration increases, while the resonant frequency and the concentration dependency are different among different types of LAs.

The above studies both used the THz polarization sensing method to distinguish the non-chiral biochemical substances. It can be seen that the optical response of the biochemical substances can be enhanced by chiral metamaterials, enabling recognition with a high accuracy due to the rich spectral information.[106,107] THz polarization detection is advantageous in high sensitivity and rich detection dimensions, providing wide applications compared with traditional sensing methods

5.3. Information Encryption and Multi-Channel Imaging

With advancements in material science and fabrication technology, metasurfaces are becoming increasingly practical and versatile. These devices now can simultaneously modulate the amplitude,[108] phase,[109] and polarization of incident waves, allowing for the generation and manipulation of vectorial optical fields.[110] Moreover, metasurfaces can flexibly manipulate polarization to ensure their efficient functionality. Anisotropic dielectric metasurfaces exhibit distinct effective refractive indexes along two birefringent principal axes, enabling improved control over polarization states. By adjusting geometric parameters along these axes and rotating the entire structure, it is possible to modulate the phase of the transmitted wave, thereby altering the polarization. Various applications such as specialized vectorial beams,[111] polarization-sensitive metalenses,[112] and holograms[113] have been successfully developed using such metasurfaces, demonstrating their potentials for creating multichannel functional devices.

For instance, Gao et al. proposed a reconfigurable chiral metasurface utilizing the phase transition properties of VO_2, capable of modulating circular dichroism (CD).[114] **Figure 10a** depicts the structural diagram of the meta-atom with incorporated VO_2. The two narrow-band CD resonances significantly broaden when the phase of VO_2 transitions from insulating to metallic, as shown in Figure 10b. By employing the inherent chiral mechanism in the metasurface, the spin-selective absorption effect of the circularly polarized wave is precisely reversed by mirroring the original meta-atom. This adjustable characteristic introduces an

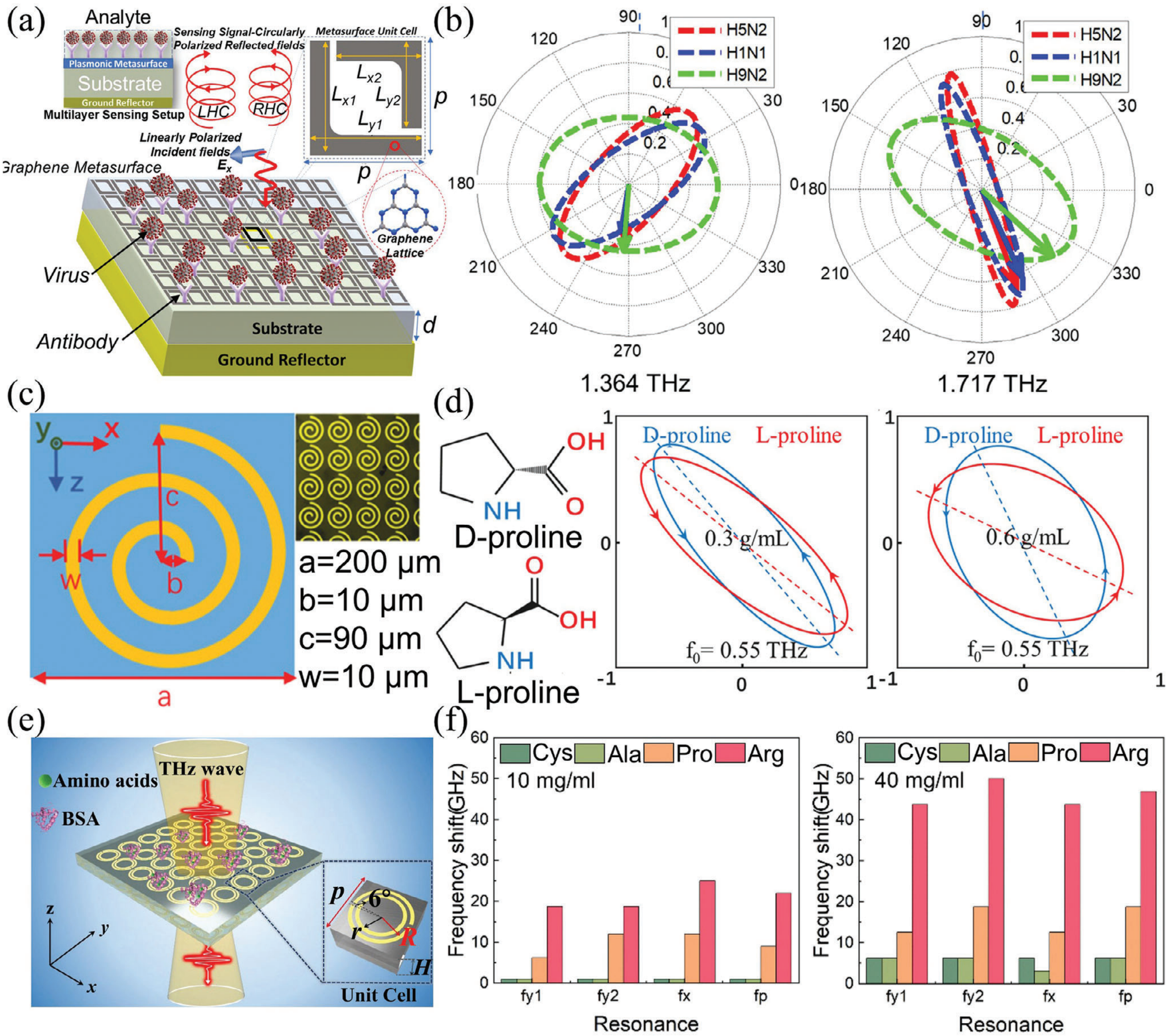

Figure 9. Polarization-specific detection. a) The chiral biosensor is constructed by a diagonally-symmetrical unit cell which consists of a graphene split ring designed with two L-shaped resonators, and the linearly polarized incident light is reflected as elliptically polarized light. b) The polarization states of the three strains of virus at two resonant frequencies 1.364 THz and 1.717 THz. Reproduced with permission.[98] Copyright 2021, Elsevier. c,d) Qualitative discrimination D- and L-enantiomers with c) geometry and dimensions of the chiral spiral metasurface and d) the structural formulas of D- and L-proline and the polarization ellipses of output THz waves of D- and L-proline at the concentration of 0.6 and 0.3 g mL^{-1} at 0.55 THz., respectively. Reproduced with permission.[100] Copyright 2021, Elsevier. e) Schematic of the metasurface consisting of double-ring arrays. f) The frequency shifts with the concentrations of 10 and 40 mg ml^{-1}, respectively. e,f) Reproduced with permission.[101] Copyright 2023, OSA.

additional level of intricacy and utility to the metasurface. Figure 10c shows the designed "C" pattern, which is arranged in two areas inside and outside the metasurface array by two different types of metasurface unit structures. The "C" part is arranged with the units high reflection, and the rest of part is arranged with units of low reflection. This characteristic enables the near-field imaging of the character "C" (Figure 10d). The proposed chiral metasurface has the potential for polarization-sensitive imaging. As shown in Figure 10e, Zhao et al. presented a novel tri-layer metallic THz metasurface for multi-channel polarization generation and phase modulation.[115] The metasurface consists of three distinct layers, each serving different purpose. The top and bottom layers are composed of orthogonal metagrating arrays, serving as precision polarization filters. This allows for dynamic control over the polarization states of the THz wave, offering unprecedented flexibility and control. The middle layer of the metasurface comprises a C-shaped antenna array, the opening angle of which is meticulously adjusted to modulate the phase of the transmitted THz wave. This phase modulation capability is crucial for beamforming and holography. Figure 10f shows the designed THz vectorial hologram metasurface with channels C1 to C8, and the phase modulations of C1 to C8 are designed

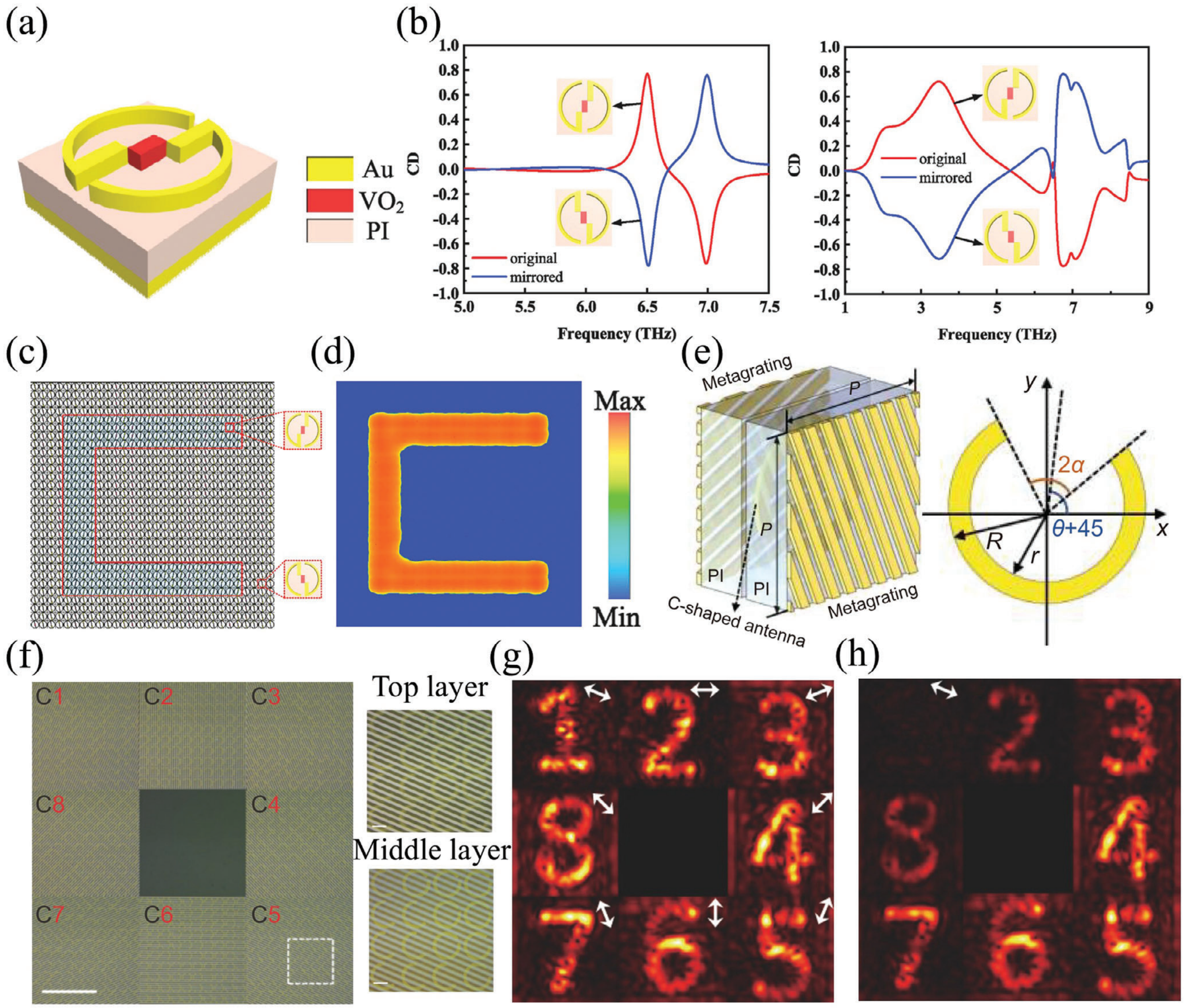

Figure 10. Polarization near-field imaging. a) The unit structure diagram of the reconfigurable chiral metasurface. b) The CD spectra with VO_2 in the insulating (left) and metallic state (right). c) The designed "C" pattern is arranged in two areas inside and outside the metasurface array by two different types of metasurface unit structures. d) The image of reflected electric field at the observation plane 20 µm away from the metasurface. a–d) Reproduced with permission.[114] Copyright 2023, Elsevier. e) The schematic of the designed tri-layer unit cell and top view of the middle layer of the unit. f) The designed THz vectorial hologram metasurface with channels C1 to C8. g) The amplitude distribution of a hologram without polarization selection and h) the amplitude distributions when an image is hidden in channel C1 with the detected polarization chosen as 67.5°. e–h) Reproduced with permission.[115] Copyright 2023, Opto-Electronic Advances.

to generate holograms of numbers 1 to 8 using the simulated annealing algorithm based on the Rayleigh–Sommerfeld diffraction theory. The image was measured without polarization selection and the images 1–8 in all channels C1 to C8 could be distinguished clearly with almost the same amplitude, as shown in Figure 10g. Figure 10h shows the result when the images of C1 are hidden with a specific linear polarization for detection, while the images in other channels can still be observed with different amplitudes. This feature offers enhanced security for information encoded in holograms, holding immense potential for future THz communication and information security applications.

In addition, Li et al. proposed a single-layer diatomic all-dielectric metasurface working in the terahertz band,[116] which can efficiently demonstrate an ability to perform bi-functional polarization switching. This unique meta-platform is constructed from a pair of anisotropic silicon pillars, each with meticulously optimized lateral dimensions and in-plane twist angles. The key aspect of this design is the ability to tailor the transmitted polarization states by arranging and combining the in-plane twist angles of half-wave plates (HWP) and quarter-wave plates (QWP). Additionally, the near-field imaging platform, an essential part of many optical systems, can be significantly improved by utilizing this diatomic design approach. The dual-functional polarization conversion capability introduces a new opportunity in the field of integrated meta-optical engineering.

The aforementioned studies are about the THz polarization metasurfaces for near-field imaging and generating holograms and their applications in information encryption and multi-channel imaging. Compared with traditional THz polarization optical elements such as waveplates and polarizers which relying on anisotropic crystal materials, metasurface polarization optical elements can manipulate the phase or amplitude of THz waves of different polarization by the well-designed micro- and nano-structures. Consequently, they possess more precise and flexible characteristics, allowing for pixelated encoding of the polarization states of THz waves at the subwavelength scale. THz metasurfaces manipulating polarization information may find tremendous applications in the fields of information encryption, multi-channel imaging, and display.

6. Conclusion and Outlook

Terahertz waves possess abundant spectral information, high penetration and non-destructive testing capabilities. The polarization analysis of terahertz waves holds significant potential for various applications such as material recognition, medical imaging, and security screening. Hence, the investigation and advancement of polarization detection technology for terahertz waves have emerged as a prominent area of research interest. New methods for processing and detecting polarization information are required to tackle the challenges of rising system miniaturization and the rapid increase in data volume. The full Stokes polarization detection provides a comprehensive characterization of the polarization state of the THz, which can reveal subtle material properties and interactions surpassing linear polarization state characterization. Although commercially available terahertz sources typically emit only linearly polarized light, the chiral THz wave and its arbitrary polarization manipulation have been realized.[117] It is significant to detect the polarization states of the generated terahertz waves for device design and optimization. In recent years, metasurfaces have demonstrated unprecedented capabilities in manipulating light propagation, providing unconventional methods for developing ultra-thin, ultra-flat, compact optical devices for polarization detection. In this review, we introduce the basic principles of polarization and the description of polarization states, including the electric vector representation of polarized light, Jones vector, Stokes vector, and Poincaré sphere. Through reviewing the research on polarization manipulation based on terahertz metasurfaces, we summarized the latest progress in utilizing terahertz metasurfaces to control and modulate the polarization state of terahertz waves, as well as in detecting polarization information. Finally, we introduced the application achievements of terahertz metasurfaces in the fields of polarization detection and imaging, including enhanced sensing, biochemical substance detection, information encryption, and multi-channel imaging. Polarized imaging provides a method of measuring and detecting the polarization information through an imaging process. These developments represent notable progress in addressing conventional constraints in polarization detection and imaging, offering an effective path for improving the integration and accuracy of polarization detection systems.

Although some exciting progress has been made in the research of polarization detection technology based on terahertz metasurfaces, challenges still exist in areas such as metasurface fabrication technology and optoelectronic integration. Utilizing dynamically tunable materials with optical properties to create terahertz metasurfaces is a highly promising technology, enabling dynamic control of polarization devices. The key to this technology lies in selecting appropriate structures and materials (such as thermal control, electrical control, etc.), and designing mechanisms capable of achieving dynamic control. Dynamic polarization metasurfaces play important roles in fields such as communication, imaging, and sensing. For example, in the field of communication, adaptive polarization control can be achieved using dynamically tunable polarization metasurfaces to enhance the stability and reliability of signal transmission; in imaging, real-time adjustable polarization characteristics of optical devices can improve imaging quality and resolution; in sensing, polarization metasurfaces can be used for highly sensitive detection of the polarization state of light, enabling more precise sensing applications. On the other hand, the development of information technology and digital technology are mutually reinforcing, which also applies to the design of terahertz polarizers. Digital technology has advantages in programmable signal processing, control, and communication, providing more flexible and precise control and adjustment of terahertz metasurfaces. In addition, digital design can also simplify the manufacturing process of terahertz metasurfaces and reduce costs. The design of polarized terahertz metasurface devices also needs to consider how to be applied to digital information systems, which have increasing demands for high-speed, high-precision data processing and transmission in fields such as communication, imaging, and sensing. The designed polarized devices need to be seamlessly integrated with digital information systems to achieve more efficient and reliable data processing and transmission. By combining polarized devices with digital signal processors, optoelectronic converters, and other digital components, a powerful polarized information processing system can be constructed to meet the needs of digital information systems.

Overall, terahertz metasurfaces have great potentials for advanced polarization manipulation and detection. With the continuous advancement of technology and increasing application demands, we believe terahertz metasurfaces will play increasingly important roles in the future, bringing more opportunities for innovation and development in high-bandwidth communication and next-generation communication technology.

Acknowledgements

Y.L., Y.X., and B.Y. contributed equally to this work. This work was supported by the National Key Research and Development Program of China (2021YFA1400601 and 2022YFA1404501), National Natural Science Fund for Distinguished Young Scholar (11925403), National Natural Science Foundation of China (12122406, 12192253, 12274239, and U22A20258), Fundamental Research Funds for the Central Universities (63241508), and 111 Project (B23045).

Conflict of Interest

The authors declare no conflict of interest.

Keywords

metasurfaces, polarization detection, polarization sensing, terahertz

Received: July 2, 2024
Revised: August 17, 2024
Published online:

[1] B. Qu, H. Zhu, J. Wang, B. Li, L. Xie, Q. Liao, L. Hu, *Appl. Energy* **2024**, *363*, 123105.
[2] Y. Peng, J. Huang, J. Luo, Z. Yang, L. Wang, X. Wu, X. Zang, C. Yu, M. Gu, Q. Hu, X. Zhang, Y. Zhu, S. Zhuang, *PhotoniX* **2021**, *2*, 12.
[3] I. Hosako, N. Sekine, M. Patrashin, S. Saito, K. Fukunaga, Y. Kasai, P. Baron, T. Seta, J. Mendrok, S. Ochiai, H. Yasuda, *Proc. IEEE* **2007**, *95*, 1611.
[4] R. Damari, O. Weinberg, D. Krotkov, N. Demina, K. Akulov, A. Golombek, T. Schwartz, S. Fleischer, *Nat. Commun.* **2019**, *10*, 3248.
[5] L. Ma, W. Shi, F. Fan, Z. Zhang, T. Zhang, J. Liu, X. Wang, S. Chang, *Chin. Opt. Lett.* **2023**, *21*, 110003.
[6] M. Beruete, I. Jáuregui-López, *Adv. Opt. Mater.* **2020**, *8*, 1900721.
[7] S. Chen, Y. Zhang, Z. Li, H. Cheng, J. Tian, *Adv. Opt. Mater.* **2019**, *7*, 1801477.
[8] Y. Sun, G. Geng, Y. Wang, Y. Zhang, Z. Li, W. Liu, H. Cheng, S. Chen, *Laser Photonics Rev.* **2024**, *18*, 2300866.
[9] E. Wang, S. Yu, T. Phan, S. Dhuey, J. Fan, *Laser Photonics Rev.* **2023**, *17*, 2200926.
[10] B. Yang, D. Ma, W. Liu, D. Y. Choi, Z. Li, H. Cheng, J. Tian, S. Chen, *Optica* **2022**, *9*, 217.
[11] J. B. Breckinridge, B. R. Oppenheimer, *Astrophys. J.* **2004**, *600*, 1091.
[12] K. Ichimoto, B. Lites, D. Elmore, Y. Suematsu, S. Tsuneta, Y. Katsukawa, T. Shimizu, R. Shine, T. Tarbell, A. Title, J. Kiyohara, K. Shinoda, G. Card, A. Lecinski, K. Streander, M. Nakagiri, M. Miyashita, M. Noguchi, C. Hoffmann, T. Cruz, *Sol. Phys.* **2008**, *249*, 233.
[13] T. Wakayama, A. Zama, Y. Higuchi, Y. Takahashi, K. Aizawa, T. Higashiguchi, *Opt. Express* **2024**, *32*, 2405.
[14] Z. Huang, Y. Zheng, J. Li, Y. Cheng, J. Wang, Z. K. Zhou, L. Chen, *Nano Lett.* **2023**, *23*, 10991.
[15] W. Xu, H. Li, S. Duan, H. Xu, C. Zheng, J. Li, C. Song, Y. Zhang, Y. Shen, J. Yao, *Nanoscale* **2023**, *15*, 17184.
[16] T. Biedenbänder, V. Aladin, S. Saeidpour, B. Corzilius, *Chem. Rev.* **2022**, *122*, 9738.
[17] Y. Li, J. Li, Y. Zhao, T. Gan, J. Hu, M. Jarrahi, A. Ozcan, *Adv. Mater.* **2023**, *35*, 2303395.
[18] P. P. Joshi, R. Li, J. L. Spellberg, L. Liang, S. B. King, *Nano Lett.* **2022**, *22*, 3180.
[19] G. L. Jones, Q. Xiong, X. Liu, B. E. Bouma, M. Villiger, *Biomed. Opt. Express* **2023**, *14*, 4609.
[20] W. Chen, J. S. Park, J. Marchioni, S. Millay, K. M. A. Yousef, F. Capasso, *Nat. Commun.* **2023**, *14*, 2544.
[21] P. Qi, J. Wang, Y. Yang, X. Yuan, T. Ye, A. Lin, Y. Zhang, Z. Huang, X. Tan, *Opt. Express* **2022**, *30*, 47264.
[22] Z. Ma, W. Zhao, J. Zhao, J. Liu, Q. Jing, J. Dou, B. Li, Y. Hu, *Opt. Laser Technol.* **2022**, *156*, 108552.
[23] S. Wang, S. Wen, Z. L. Deng, X. Li, Y. Yang, *Phys. Rev. Lett.* **2023**, *130*, 123801.
[24] I. Wilke, J. Monahan, S. Toroghi, P. Rabiei, G. Hine, *Sci. Rep.* **2024**, *14*, 822.
[25] W. Zhu, X. Liang, W. Xie, H. Zheng, Y. Zhong, J. Tang, J. Yu, Z. Chen, *Laser Photonics Rev.* **2024**, *18*, 2301030.
[26] W. Xiao, M. Zhang, R. Zhang, C. Zhang, L. Zhang, *Appl. Phys. Lett.* **2023**, *122*, 061105.
[27] L. Liu, W. Liu, F. Wang, X. Peng, D. Y. Choi, H. Cheng, Y. Cai, S. Chen, *Light: Sci. Appl.* **2024**, *13*, 131.
[28] J. Li, C. Zheng, J. Li, G. Wang, J. Liu, Z. Yue, X. Hao, Y. Yang, F. Li, T. Tang, Y. Zhang, Y. Zhang, J. Yao, *Photonics Res.* **2021**, *9*, 1939.
[29] W. Liu, Z. Li, M. A. Ansari, H. Cheng, J. Tian, X. Chen, S. Chen, *Adv. Mater.* **2023**, *35*, 2208884.
[30] Y. Jiang, W. Liu, Z. Li, D. Y. Choi, Y. Zhang, H. Cheng, J. Tian, S. Chen, *Adv. Opt. Mater.* **2023**, *11*, 2202186.
[31] Y. Intaravanne, R. Wang, H. Ahmed, Y. Ming, Y. Zheng, Z. K. Zhou, Z. Li, S. Chen, S. Zhang, X. Chen, *Light: Sci. Appl.* **2022**, *11*, 302.
[32] S. Gao, C. Zhou, W. Liu, W. Yue, S. Chen, S. S. Lee, D. Y. Choi, Y. Li, *Laser Photonics Rev.* **2022**, *16*, 2100603.
[33] J. Cheng, Z. Li, D. Y. Choi, S. Yu, W. Liu, H. Wang, Y. Zhang, H. Cheng, J. Tian, S. Chen, *Adv. Opt. Mater.* **2022**, *11*, 2202329.
[34] M. Geng, X. Yang, H. Chen, X. Bo, M. Li, Z. Liu, W. Liu, *Photonics Res.* **2023**, *11*, 129.
[35] Q. Li, C. Wu, Z. Zhang, S. Zhao, B. Zhong, S. Li, H. Li, L. Jin, *IEEE Trans. Antennas Propag.* **2022**, *71*, 774.
[36] X. Xue, B. Xu, B. Wu, X. Wang, X. Yu, L. Lin, H. Li, *Opt. Express* **2022**, *30*, 20389.
[37] H. Xue, X. Wu, X. Cui, M. Chang, H. Liu, L. Li, T. Cui, *IEEE Trans. Microw. Theory* **2022**, *70*, 4449.
[38] I. Kim, J. Jang, G. Kim, J. Lee, T. Badloe, J. Mun, J. Rho, *Nat. Commun.* **2021**, *12*, 3614.
[39] Q. Wei, L. Huang, R. Zhao, G. Geng, J. Li, X. Li, Y. Wang, *Adv. Opt. Mater.* **2022**, *10*, 2102166.
[40] J. Li, W. Liu, H. Xu, Z. Huang, J. Wang, J. Wen, J. Yang, J. Guan, S. Wang, A. Alù, Z. K. Zhou, S. Chen, *Laser Photonics Rev.* **2024**, *18*, 2300729.
[41] L. Zhang, S. Chang, X. Chen, Y. Ding, M. T. Rahman, Y. Duan, M. Stephen, X. Ni, *Laser Nano Lett.* **2023**, *23*, 51.
[42] A. H. Dorrah, N. A. Rubin, A. Zaidi, M. Tamagnone, F. Capasso, *Nat. Photonics* **2021**, *5*, 287.
[43] C. He, H. He, J. T. Chang, B. G. Chen, H. Mai, M. J. Booth, *Light: Sci. Appl.* **2021**, *10*, 194.
[44] M. Solomon, J. Hu, M. Lawrence, A. Garcia-Etxarri, J. A. Dionne, *ACS Photonics* **2019**, *6*, 43.
[45] R. C. Jones, *J. Opt. Soc. Am.* **1941**, *31*, 488.
[46] H. Hurwitz, R. C. Jones, *J. Opt. Soc. Am.* **1941**, *31*, 493.
[47] C. Menzel, C. Rockstuhl, F. Lederer, *Phys. Rev. A* **2010**, *82*, 053811.
[48] G. G. Stokes, *Trans. Camb. Phil. Soc.* **1852**, *9*, 399.
[49] H. G. Berry, G. Gabrielse, A. E. Livingston, *Appl. Opt.* **1977**, *16*, 3200.
[50] S. Y. Lu, R. A. Chipman, *Opt. Commun.* **1998**, *146*, 11.
[51] M. J. Padgett, J. Courtial, *Opt. Lett.* **1999**, *24*, 430.
[52] G. Li, S. Chen, N. Pholchai, B. Reineke, P. W. H. Wong, E. Y. B. Pun, K. Cheah, T. Zentgraf, S. Zhang, *Nat. Mater.* **2015**, *14*, 607.
[53] M. V. Berry, *Proc. R. Soc. A* **1984**, *392*, 45.
[54] L. L. Huang, X. Z. Chen, H. Muehlenbernd, G. X. Li, B. F. Bai, Q. F. Tan, G. Jin, T. Zentgraf, S. Zhang, *Nano Lett.* **2012**, *12*, 5750.
[55] C. Sonnichsen, T. Franzl, T. Wilk, G. von Plessen, J. Feldmann, O. Wilson, P. Mulvaney, *Phys. Rev. Lett.* **2022**, *88*, 077402.
[56] S. Campione, L. Basilio, L. K. Warne, M. B. Sinclair, *Opt. Express* **2015**, *23*, 2293.
[57] S. M. Hein, H. Giessen, *Phys. Rev. Lett.* **2013**, *111*, 026803.
[58] T. Cao, C. W. Wei, Y. Li, *Opt. Mater. Express* **2016**, *6*, 303.
[59] S. Yin, Y. Chen, B. Quan, S. Liu, W. Huang, M. Liu, W. Zhang, J. Han, *Nanophotonics* **2023**, *12*, 1317.
[60] T. Ma, J. Tian, J. Li, *Opt. Commun.* **2023**, *532*, 129216.
[61] J. Li, J. Li, C. Zheng, Y. Yang, Z. Yue, X. Hao, H. Zhao, F. Li, T. Tang, L. Wu, J. Li, Y. Zhang, J. Yan, *Opt. Express* **2021**, *29*, 28329.
[62] C. Zheng, J. Li, S. Wang, J. Li, M. Li, H. Zhao, X. Hao, H. Zang, Y. Zhang, *Appl. Phys. Lett.* **2021**, *118*, 051101.
[63] B. Yang, M. Ouyang, H. Ren, C. Ma, Y. Zhao, Y. Zhang, Y. Zhang, Y. Fu, *Coatings* **2022**, *12*, 736.
[64] F. Yang, H. Li, C. Song, J. Li, J. Li, C. Zheng, Z. Yue, X. Ding, Y. Zhang, J. Yao, *Optik* **2022**, *262*, 169305.

[65] M. Kobachi, F. Miyamaru, T. Nakanishi, K. Okimura, A. Sanada, Y. Nakata, *Adv. Opt. Mater.* **2022**, *10*, 2101615.
[66] T. Lv, Y. Li, C. Qin, J. Qu, B. Lv, W. Li, Z. Zhu, Y. Li, C. Guan, J. Shi, *Opt. Express* **2022**, *30*, 5439.
[67] X. Jiang, Y. Ji, F. Fan, H. Zhao, S. Jiang, J. Cheng, M. Wu, J. Xin, S. Chang, *Opt. Lett.* **2023**, *48*, 1682.
[68] F. Fan, D. Zhao, Z. Tan, Y. Ji, J. Cheng, S. Chang, *Adv. Opt. Mater.* **2021**, *9*, 2101097.
[69] X. Luo, J. Luo, F. Hu, G. Li, *Chin. Phys. B* **2023**, *32*, 027801.
[70] Li J., Fu J., Liao Q., Ke S., *J. Opt. Soc. Am. B* **2019**, *36*, 2492.
[71] W. Yang, Z. Li, M. Liu, Y. Zhang, H. Zhang, *Appl. Phys. Express* **2023**, *16*, 012011.
[72] F. Hu, T. Zou, B. Quan, X. Xu, S. Bo, T. Chen, L. Wang, C. Gu, J. Li, *Opt. Commun.* **2014**, *332*, 321.
[73] H. Zhang, L. Si, T. Ma, L. Dong, R. Niu, X. Bao, H. Sun, J. Ding, *Electronics* **2022**, *11*, 4195.
[74] A. Teber, *Adv. Theor. Simul.* **2023**, *7*, 2300918.
[75] B. Yang, M. Ouyang, H. Ren, J. Wu, Y. Zhang, Y. Fu, *Photonics* **2023**, *10*, 100.
[76] Z. Chen, H. Tang, Z. Chen, T. Shen, H. Zhang, *Opt. Mater.* **2024**, *147*, 114639.
[77] R. Wang, J. Han, J. Liu, H. Tian, W. Sun, L. Li, X. Chen, *Opt. Lett.* **2020**, *45*, 3506.
[78] Z. Jiang, M. Chao, Q. Liu, B. Cheng, G. Song, J. Liu, *Opt. Lasers Eng.* **2024**, *174*, 107816.
[79] Y. Zhang, J. Jin, M. Pu, Q. He, Y. Guo, X. Li, X. Ma, X. Luo, *Phys. Status Solidi-R.* **2020**, *14*, 2000044.
[80] S. Zhou, K. Xi, S. Zhuang, Q. Cheng, *Nanomaterials* **2021**, *11*, 2774.
[81] T. S. Nowack, Y. D. Shah, I. Escorcia, J. P. Grant, M. Kenney, V. Pusino, D. Faccio, E. Wasige, D. R. S. Cumming, *Opt. Lett.* **2022**, *47*, 4199.
[82] H. Li, S. Duan, C. Zheng, H. Xu, J. Li, C. Song, F. Yang, W. Shi, Y. Zhang, Y. Shen, J. Yao, *Nanophotonics* **2023**, *12*, 3359.
[83] X. Zhang, Y. Xu, W. Yue, Z. Tian, J. Gu, Y. Li, R. Singh, S. Zhang, J. Han, W. Zhang, *Adv. Mater.* **2015**, *27*, 7123.
[84] Z. Min, J. S. Li, *Opt. Commun.* **2022**, *511*, 127997.
[85] Z. Jiang, J. Lu, J. Fan, J. Liang, M. Zhang, H. Su, L. Zhang, H. Liang, *Laser Photonics Rev.* **2023**, *17*, 2200484.
[86] W. Xu, H. Li, H. Xu, Q. Tan, C. Song, J. Yao, *J. Opt.* **2023**, *25*, 125103.
[87] C. Zheng, J. Liu, H. Li, M. Wang, H. Zang, Y. Zhang, J. Yao, *Photonics Res.* **2023**, *11*, 2256.
[88] C. Zheng, H. Li, H. Zang, J. Yao, *Opt. Laser Technol.* **2024**, *170*, 110210.
[89] H. Li, C. Zheng, S. Duan, J. Li, H. Xu, Y. Li, C. Song, F. Yang, Z. Yue, W. Shi, Y. Zhang, Y. Shen, J. Yao, *Laser Photonics Rev.* **2023**, *17*, 2300428.
[90] X. Tian, A. Ma, H. Huang, K. Ma, H. Guo, *Phys. Scr.* **2024**, *99*, 025531.
[91] J. Li, G. Wang, Z. Yue, J. Liu, J. Li, C. Zheng, Y. Zhang, Y. Zhang, J. Yao, *Opto-Electron. Adv.* **2022**, *5*, 210062.
[92] J. Peng, J. Y. Hou, T. T. Tang, J. Li, Z. Chen, *Phys. Status Solidi B* **2022**, *259*, 2200114.
[93] S. Asgari, N. Granpayeh, T. Fabritius, *Opt. Commun.* **2020**, *474*, 126080.
[94] F. Fan, C. Zhong, Z. Zhang, S. Li, S. J. Chang, *Nanoscale Adv.* **2021**, *3*, 4790.
[95] K. V. Sreekanth, Y. Alapan, M. ElKabbash, E. Ilker, M. Hinczewski, U. A. Gurkan, A. D. Luca, G. Strangi, *Nat. Mater.* **2016**, *15*, 621.
[96] L. Liu, T. Li, Z. Liu, F. Fan, H. Yuan, Z. Zhang, S. Chang, X. Zhang, *Biomed. Opt. Express* **2020**, *11*, 2416.
[97] C. Zhong, F. Fan, Z. Zhang, H. Liu, S. Chang, *Opt. Lasers Eng.* **2022**, *149*, 106798.
[98] Y. Hao, R. Yang, *Opt. Express* **2023**, *31*, 3059.
[99] W. J. Choi, K. Yano, M. Cha, F. M. Colombari, J. Y. Kim, Y. Wang, S. H. Lee, K. Sun, J. M. Kruger, A. F. de Moura, N. A. Kotov, *Nat. Photonics* **2022**, *16*, 366.
[100] Z. Zhang, T. Zhang, F. Fan, Y. Ji, S. Chang, *Sens. Actuators, A* **2022**, *338*, 113499.
[101] M. Amin, O. Siddiqui, H. Abutarboush, M. Farhat, R. Ramzan, *Carbon* **2021**, *176*, 580.
[102] Z. Zhang, C. Zhong, F. Fan, G. Liu, S. Chang, *Sens. Actuators, B* **2021**, *330*, 129315.
[103] Z. Zhang, F. Fan, W. Shi, T. Zhang, S. Chang, *Biomed. Opt. Express* **2022**, *13*, 209.
[104] W. Shi, F. Fan, T. Zhang, J. Liu, X. Wang, S. Chang, *Biomed. Opt. Express* **2023**, *14*, 1096.
[105] J. Yang, T. Wang, G. Fang, L. Qi, X. Chen, *Opt. Laser Technol.* **2024**, *172*, 110487.
[106] W. N. Shi, Y. M. Wang, F. Fan, J. Y. Liu, J. Cheng, X. Wang, S. J. Chang, *Nanoscale* **2023**, *15*, 14146.
[107] J. Yang, T. W. Wang, G. Fang, L. Qi, X. Q. Chen, *Opt. Laser Technol.* **2024**, *172*, 110487.
[108] S. Tao, Z. Shen, H. Yu, H. Wang, S. Ge, W. Hu, *Opt. Lett.* **2022**, *47*, 1650.
[109] Z. Shen, S. Zhou, S. Ge, W. Duan, L. Ma, Y. Lu, W. Hu, *Opt. Express* **2019**, *27*, 8800.
[110] H. Xu, G. Hu, L. Han, M. Jiang, Y. Huang, Y. Li, X. Yang, X. Ling, L. Chen, J. Zhao, C. Qiu, *Adv. Opt. Mater.* **2019**, *7*, 1801479.
[111] C. Yan, X. Li, M. Pu, X. Ma, F. Zhang, P. Gao, Y. Guo, K. Liu, Z. Zhang, X. Luo, *ACS Photonics* **2019**, *6*, 628.
[112] X. Zang, H. Ding, Y. Intaravanne, L. Chen, Y. Peng, J. Xie, Q. Ke, A. V. Balakin, A. P. Shkurinov, X. Chen, Y. Zhu, S. Zhuang, *Laser Photonics Rev.* **2019**, *13*, 1900182.
[113] Q. Song, A. Baroni, R. Sawant, P. Ni, V. Brandli, S. Chenot, S. Vézian, B. Damilano, P. . Mierry, S. Khadir, P. Ferrand, P. Genevet, *Nat. Commun.* **2020**, *11*, 2651.
[114] P. Gao, C. Chen, Y. Dai, X. Wang, H. Liu, *Opt. Mater.* **2023**, *145*, 114448.
[115] H. Zhao, X. Wang, S. Liu, Y. Zhang, *Opto-Electron. Adv.* **2023**, *6*, 220012.
[116] H. Li, W. Xu, H. Xu, C. Song, Q. Tan, J. Yao, *J. Opt.* **2024**, *26*, 035102.
[117] C. Q. Liu, S. Wang, S. Zhang, Q. N. Cai, P. Wang, C. Tian, L. Zhou, Y. Wu, Z. S. Tao, *Adv. Photonics* **2021**, *3*, 056002.

Yongliang Liu is a Ph.D. student at the School of Physics, Nankai University, China. He received his M.E. degree in instrumentation engineering in 2019 from North University of China. His current research focuses on the application of terahertz metasurfaces in optical field manipulation.

Yifei Xu is a Ph.D. student at the School of Physics, Nankai University, China. He received his M.S. degree in electronic information in 2023 from Shenzhen University of China. His current research focuses on the application of terahertz metasurfaces in optical field manipulation.

Bo Yu is a Ph.D. student at the School of Physics, Nankai University, China. He received his B.E degree of microelectronics science and engineering in 2022 from Nankai University of China. His current research focuses on the application of terahertz metasurfaces in optical field manipulation.

Shuqi Chen is a professor at the Key Laboratory of Weak Light Nonlinear Photonics, Ministry of Education, School of Physics and TEDA Institute of Applied Physics, Nankai University, China. He received his joint training Ph.D. degree from the University of Arizona, USA, and Nankai University, China, in 2009. His current research interests include nonlinear optics, phononics and acoustics metasurfaces, and subwavelength electromagnetics.